3D PRINTING OF LARGE-SCALE INTEGRATED MICROFLUIDIC DEVICES

A THESIS
SUBMITTED TO THE FACULTY OF
UNIVERSITY OF MINNESOTA
BY

SARAVANAN SUJIT KAARTHIK

IN PARTIAL FULFILLMENT OF THE REQUIREMENTS
FOR THE DEGREE OF
MASTER OF SCIENCE

ADVISOR: DR. MICHAEL C. McALPINE

2024

Acknowledgments

I am grateful to many people and labs who played a crucial role in my thesis journey, helping me learn and gain valuable experience.

I want to express my sincere appreciation to my advisor, Dr. Michael McAlpine, for consistently providing insight, guidance, and support throughout my Master's thesis.

I extend my gratitude to my examining committee members, Dr. Sungyon Lee and Dr. David Wood, for dedicating their time and sharing valuable insights during the review of my thesis and defense.

I extend my thanks to my lab's manager, Melanie Burns, for maintaining a positive atmosphere in the lab and taking care of non-research essentials during my time here.

I extend my thanks to Dr. Fujun Wang for training me, setting up the foundation for the project, and building the flow control setup used in this work. Special thanks to my lab mates who contributed various insights over the past two years, helping me progress in my research. I am especially grateful to Daniel Ng, Hyunjun Kim, and Dr. Jiyong Lee for their consideration in allowing me to use the Aerotech 3D printer whenever I needed. I also appreciate Adarsh Somayaji for providing important inputs on printing silicone with fillers.

I would like to acknowledge my collaborators from the Hunter Lab, Mitchell Penningroth and Kayla Hoffman, for their contribution to growing the YFP-stained PA14 liquid culture used in the microfluidic device biofilm experiments. Thanks also to my collaborators from GRIP for engaging in fruitful discussions to enhance the Multiplexed Microfluidic Dispenser.

Special thanks to my friend, Harshitha, for teaching me how to use Adobe Illustrator to create visual aids for my thesis. Her help was invaluable.
I also want to thank my friends in Minneapolis who were crucial to my mental health during this journey, especially Deepti, for always engaging in discussions about my research and my roommates Koushik and Thiru, without whose laptop I wouldn't have been able to write this thesis.

Most importantly, I would like to thank my parents, M. Azhaguvelammal and K.P. Saravanan. Without their sacrifices and hard work, none of this would be possible.

Abstract

The ability to manufacture large-scale integrated microfluidic devices (mLSI) in an automated fashion with high throughput could impact numerous areas, including single-cell assays, drug discovery, and multi-sample analysis of human fluids. Conventional microfluidics fabrication is labor-intensive and requires the use of specialized facilities. Our group previously pioneered a method to 3D print microfluidic channels and valves by extruding silicone filaments in angular stacks. This technique faced limitations in scaling due to slow printing speed (1 mm/s) and inability to generate multiplexed flows. Here, we present an approach to 3D print mLSI devices that introduces an innovative method to reinforce channels locally and reduce the printing time 20-fold by doubling the extrusion diameter of the filaments. This allows for the incorporation of a Boolean design strategy that requires specific valves to remain open when actuated. This work paves the way for point-of-need mLSI production for medical diagnostics and disease detection.

Table of Contents

List of Figures

CHAPTER 1

INTRODUCTION

1.1. Project Motivation & Objective

Microfluidic large-scale integration (mLSI) has transformed the landscape for many applications[1] such as biological screening,[2] cell culture,[3] and DNA-based storage systems[4] by increasing the processing power of these devices. The ability to control an exponential number of flows distinctly was achieved by adopting a Boolean strategy to sequentially activate pneumatically actuated microfluidic valves that can control the flow with an optimal number of inputs.[5] The appeal of microfluidics lies in its ability to work with minimal volumes of reagents and samples,[6] resulting in cost-cutting advantages and contributing to the efficiency of various applications. By increasing the processing power of these devices through large-scale integration, extremely high throughput can be achieved by parallelization of processes,[7] increasing the number of iterations,[8] and development of multiplexed flows. This advantage positions mLSI as a pivotal innovation in driving advancements in various fields that leverage the benefits of microfluidics, enabling researchers to push boundaries.

Pneumatically actuated valves are the cornerstone of microfluidic automation. They function by exploiting the elastomeric nature of the microfluidic channels and stop the flow in them by creating a pinching mechanism. A robust channel, known as the control channel, is aligned around the microfluidic channel and is pressurized with air. When the

stress created by the air pressure is high enough to deform the walls of the microfluidic channel, it causes the cross-section to gradually reduce to zero, creating a resistance to a pressure-driven flow, causing it to stop. These types of valves are essential autonomous components in various microfluidic technologies and have been used to enable the automation of microfluidic devices. They can also be actuated serially in a peristaltic sequence to function as a pump.[9]

The microfluidic chips that these valves control can perform many functions required for biological applications, such as mixing,[10] cell sorting,[11] and droplet generation.[12] However, to enable large-scale integration of these functions on a single chip and fully capitalize on the benefits of microfluidic technology, linearly increasing the number of valves to control each channel is not a practical option. The infeasibility stems from the significant increase in the amount of peripheral equipment required to control the valves and the challenges in terms of interfacing the microfluidic device with a multitude of pneumatic connections.[5] To address this challenge, a method of utilizing binary combinations of distinct valve arrays was developed, exponentially reducing the number of pneumatic connections required for controlling a microfluidic chip. This concept is known as microfluidic large-scale integration (mLSI) or microfluidic multiplexing,[5] analogous to large-scale integration in electronics.

PDMS (polydimethylsiloxane), an elastomer, has emerged as a standout material for manufacturing mLSI devices, primarily due to advances in microfabrication methods that

have been established as the standard to fabricate them.[13] It can also be easily modified chemically and physically to improve its properties based on the application's necessities.[14] However, conventional microfabrication techniques, like soft lithography, present certain challenges, including the need for a cleanroom environment, alignment issues while fabricating microfluidic channels onto prefabricated chips or pre-existing features, and are labor-intensive processes.[15] 3D printing is rising as a promising alternative for creating microfluidic chips[16] whilst overcoming these challenges. Different techniques such as stereolithography,[17,18] poly-jet printing,[19] and direct-ink-writing[20,21] are leveraged to fabricate microfluidic devices that possess different advantages such as improved resolution or better integration with existing experimental set-ups. Moreover, the adaptability of 3D printing allows for the rapid prototyping of microfluidic devices, facilitating iterative design improvements.[22] This advancement is beneficial in research and development, where rapid modifications and testing are essential.

The McAlpine research group developed a method to directly "write" microfluidic devices onto any substrate.[21] This method follows an extrusion-based approach to 3D print RTV silicone which is a one-part sealant that requires moisture in the atmosphere as a second component for condensation curing.[23] The material is shear thinning, with a high yield strength, allowing the 3D printing of self-supporting walls that resist the force of gravity to create hollow microfluidic channels. The one-part silicone is hydroxy end-blocked and has an acetoxy group. The ambient moisture hydrolyzes the acetoxy group to

allow crosslinking to occur[23] to produce elastic channels after the 3D printed structures cure for 24 hours. Apart from overcoming the challenges posed by soft lithography as mentioned earlier, this technique also possesses the following advantages:

- Optimizing the space on pre-existing chips where microfluidic channels printed only at the required locations compared to a slab of PDMS occupying unnecessary room.
- Incorporating microfluidic channels of different materials and different heights onto the same substrate, which can be difficult with conventional microfabrication.
- Fabricating microfluidic channels onto both plane and curved surfaces opens potential avenues such as directly printing microfluidic devices on human skin and creating state-of-the-art medical devices.

This work aims to extend the 3D printing methodology developed by the McAlpine research group to enable the fabrication of large-scale integrated microfluidic devices. This advancement involves conformally printing a control channel, which is an array of valves, over multiple flow channels that can simultaneously allow some of them to be closed and some of them to be open as per the requirement of the application. Development of these high-density automated devices includes optimization of the 3D printing process, calculating the toolpath to 3D print a channel conformally over multiple flow channels, and conceptualizing a strategy to not to close some of the flows that an

actuated control channel overlaps. The method of direct-ink-writing also allows for the enhancement of the channels' mechanical properties by mixing RTV silicone with additives. Finally, these principles were applied to design and 3D print devices for two applications:

- A lab-on-a-chip device used to study the effect of plasma-activated water on *Pseudomonas aeruginosa* (PA14) biofilms under flow conditions, which includes a multiplexed fluid inlet system, a gradient generator to produce different concentrations of plasma-activated water to treat the biofilm, and a series of culture chambers to observe the biofilms through a microscope.
- A fluid dispensing device that directs twelve different flows into four outlets that lead to a graphene biosensor with four different sensing regions. This system functionalizes the graphene biosensor through the application of reagents and various biomolecules to create a multiplexed sensor for the detection of four different diseases.

1.2. Related Work

3D printing is growing in relevance as an alternative to solve the challenges posed by microfabrication techniques for the manufacturing of microfluidic devices.[16] 3D printing technologies that have been successful in creating automated microfluidic devices include

stereolithography, poly-jet printing,[28] and direct-ink-writing.[21] Amongst the methods for 3D printing microfluidic autonomous components, stereolithography has taken the biggest strides in terms of producing the highest density of valves on a device[25,26] with the highest resolution.[27]

Stereolithography is an additive manufacturing technique that constructs a required 3D shape layer by layer by solidification of photopolymers that are contained in a vat.[25] Unlike extrusion-based 3D printing technologies, where a nozzle moves along the designated toolpath, stereolithography controls the movement of a source of light to cure the photopolymer and achieve the desired shape. Initially, only UV light was used for photopolymerization.[29] However, the technology has progressed to use light in the visible spectrum as well.[30] This technique has been successfully implemented to create automated microfluidic devices with high density and throughput.

The Folch group utilized a commercially available stereolithography printer to create a membrane-style microfluidic valve[31] using WaterShed XC 11122 resin. This valve consists of a control channel that is pressurized with air that is layered below the flow channel, and the diameter of the laser controls the thickness of the interface between them. Once the channels are printed, the uncured resin in the cavity is rinsed out to create the hollow microfluidic components. The resolution of this work was improved to reduce the membrane thickness from more than 100 μm to 25 μm and control channel diameter from close to 10 mm to 1 mm. These resolution and printability limitations were overcome by altering the design to feature a "bowl-shaped valve seat" and using PEG-

DA-258 as the photopolymer. These changes allowed the printing of a microfluidic device consisting of an array of 64 valves of diameter 500 μm.[25]

The Nordin group successfully constructed microfluidic valves using stereolithography by photoreduction of an image projected by a UV-illuminated dynamic mask[26] for curing the photopolymer. In this design, where the control chamber is placed above the flow channel, the thickness of the interface between them is controlled by the exposure time of the light. This method led to high-resolution channels with cross-sectional dimensions as small as 250 μm and valves of diameter 2 mm to 3 mm. The resolution of this method was dramatically improved to valve dimensions of up to 15 μm ×15 μm[32] by altering their 3D printing methodology to enhance the precision beyond that of the 3D printer by spatially controlling the exposure time of the resin across each layer. This improvement led to the creation of an extremely high-density microfluidic device (70 squeeze valves within an area of 2.2 mm × 1.1 mm), which functioned as a 10-stage, 2-fold serial diluter.

1.3. Project Outline

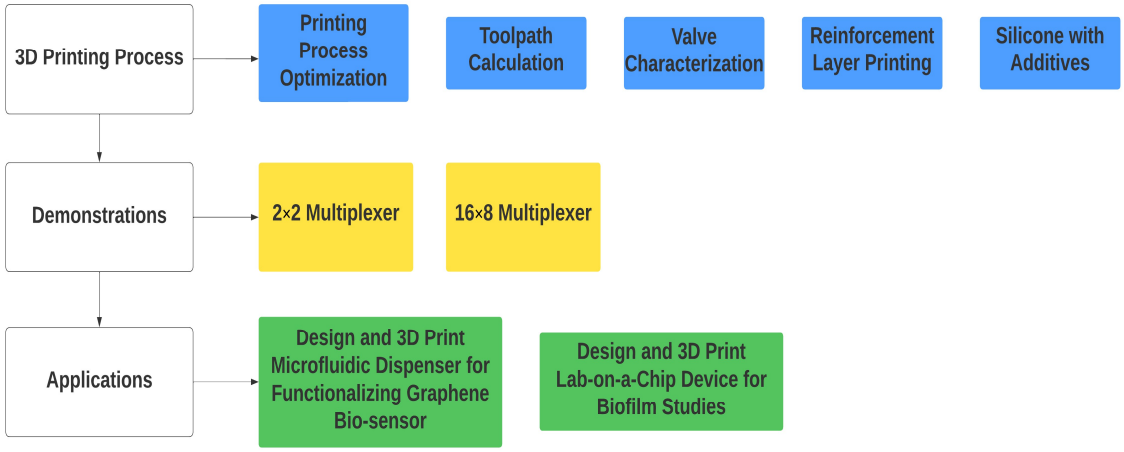

Figure 1. Project goals overview

In this section, the outline of the project has been laid out to highlight the different goals and their purpose over the period of the conducted work and how they are necessary to improve the current fabrication methodology to create large-scale integrated microfluidic devices. First, it was necessary to improve the printing speed from the existing protocol that had been established. This process was a necessity as the printing material, RTV silicone, cures over time in ambient conditions, which degrades its printability. Once the printing process parameters were improved and established, they were used for conformally 3D printing control channels over multiple flow channels of different dimensions to demonstrate the scaling up of the existing valve design developed by the McAlpine research group. These valves were then characterized using the flow control setup to identify the working pressures of the valves for different channel dimensions.

Once the operating pressure range of the valves was identified, a method of reinforcing flow channels at sites where the control channels overlap them was developed to prevent the channel from closing due to the applied pressure. This technique enabled the direct-ink-writing of multiplexed devices. Next, a method of improving the burst pressure of the channels using additives in silicone was attempted. These printing process parameters were utilized to 3D print a 2×2 multiplexer and a 16×8 multiplexer to demonstrate the proof of concept. Lastly, two devices were designed, and 3D printed using the principles of the conducted research to create a lab-on-a-chip device to study bacterial biofilms and a microfluidic dispensing device to functionalize a graphene biosensor for the detection of multiple diseases.

CHAPTER 2

BACKGROUND RESEARCH

2.1. Direct-ink-writing of Silicone

Direct-ink-writing is an additive manufacturing technique that implements an extrusion-based method to push pressurized viscoelastic material out of a nozzle.[33] The movement of the nozzle is controlled in a 3D space to create a stack of filaments that form a 3D shape. The 3D printed shape then requires curing in ambient conditions or some post-processing methods such as heating or UV light exposure.[34] The rheological properties of the ink play a crucial role in this manufacturing method as it requires the material to generally be a shear-thinning liquid with a yield stress value low enough to be extruded out of a nozzle but also high enough to retain its shape after printing.[35] The fact that the curing occurs after completely printing the shape allows crosslinking between the filaments, which is similar to the 3D printing of thermoplastic materials.[36]

The properties of the elastomeric polymers used in direct-ink-writing can also be improved by adding fillers such as particles or fibers. This can be done either to alter the rheology of the ink by adding particles such as fumed silica[37] or to enhance the strength and stiffness of the elastomers post-curing by adding carbon[38] or glass fibers.[39]

This method of 3D printing is advantageous over other methods, such as stereolithography, for the creation of microfluidic devices as it does not require any sacrificial materials that will contaminate the channels or require any complicated processes such as melting or sintering before or during the 3D printing process. All that is required is for the polymer to be able to be extruded through a nozzle at room temperature and maintain its shape.

2.2. Self-Supporting Microfluidic Channels

The McAlpine research group leveraged these principles to create hollow 3D structures that do not require a supporting material during the 3D printing process. Silicone walls are printed at an angle that allows them to be printed based on the maximum bending moment at the root of the wall caused by gravitational loading.[21] These silicone walls printed at supplementary angles give rise to hollow structures that can be printed without requiring any supporting material (Fig.2.A.).

For direct-ink-writing these structures, it is necessary for the yield stress of the material to be strong enough to resist deformation due to its own weight[40,41] and normally requires sacrificial materials[42] to overcome this challenge. A cantilever beam model was used to analyse the distribution of bending moment due to gravitational loading across the printed silicone wall. This analysis established that the yield stress of the silicone was

high enough to print silicone walls up to an angle of 37°, below which they start to collapse, and this theory was also experimentally validated (Fig.2.B.). The yield stress was also low enough to be extruded through a 32GA nozzle of internal diameter 0.1 mm using a pressure dispensing system at a pressure of 25 psi amplified seven-fold for a printing speed of 1 mm/s.

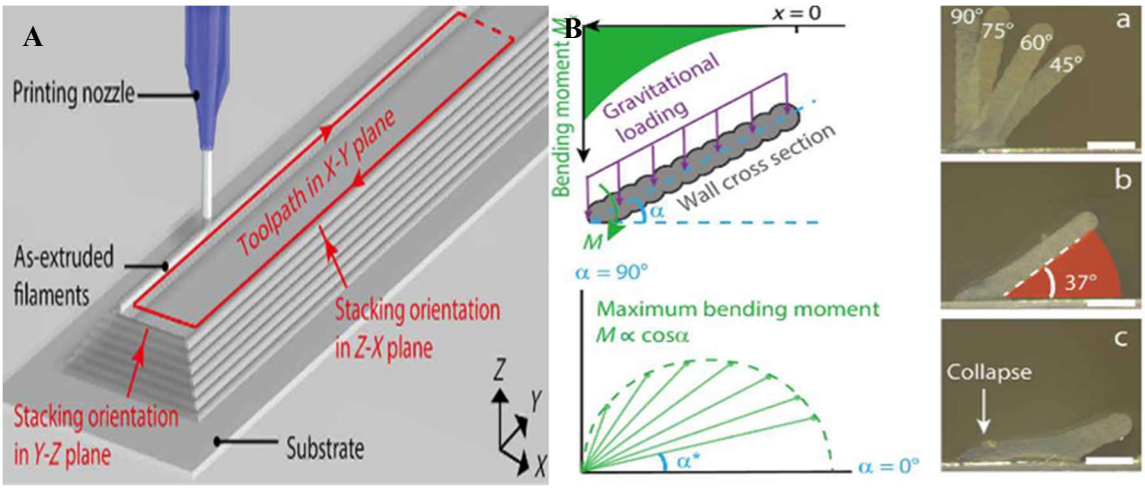

Figure 2. Direct-ink-writing of self-supporting microfluidic devices. (A) Layer-by-layer building of toolpath [21] (B) Limiting angle of self-supporting silicone walls[21]

The material used to print these channels, RTV silicone, is a one part silicone that undergoes condensation curing using moisture in the atmosphere as the second component[23]. This allows the microfluidic channels that are printed to cure in ambient conditions without any post-processing methods such as thermal or UV curing.

Toolpaths were designed for the trajectory of the 3D printing nozzle (Fig.2.A.) to create microfluidic channels and components such as mixers, valves, and pumps. 3D printing these channels on curved substrates was also demonstrated to showcase the potential of the method to fabricate microfluidic devices directly onto surfaces such as the human hand to create large-scale medical devices.

2.3. Quake Valve Design and DIW Microfluidic Valve

The need to control flow in the microscale led to the development of a pneumatically controlled microfluidic valve. A method was conceived using multilayer soft lithography to fabricate channels that are conformally placed over PDMS based microfluidic conduits. These sealed channels are actuated with air to stop the flow below them.[24] The interface between both channels is deformed by the stress induced by the air pressure initiating the valve mechanism.

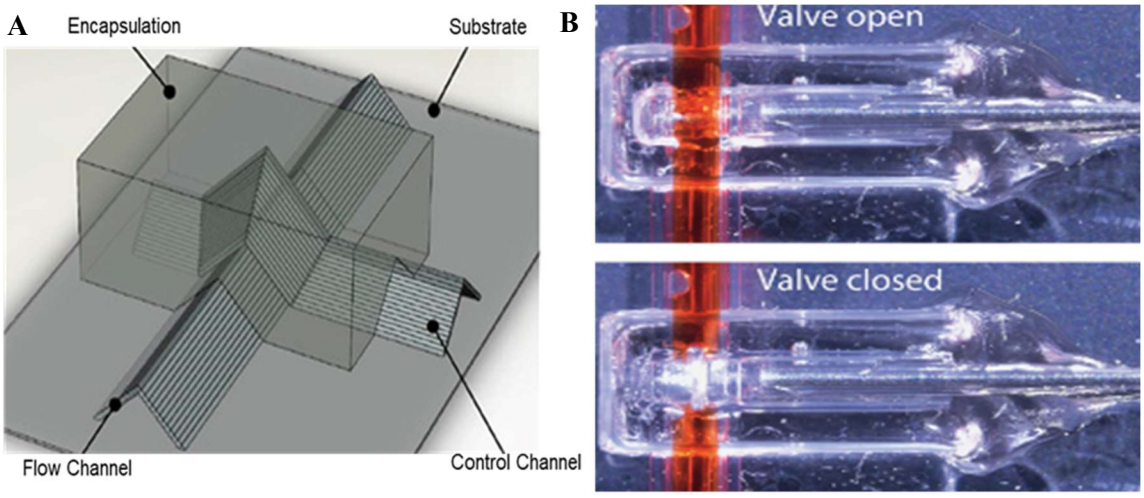

Figure 3. Microfluidic Valve by Direct-ink-writing (A) Illustration of the valve [21], (B) Working of the valve [21]

This principle was adopted by the McAlpine research group while trying to replicate the "Quake-style" valve for direct-ink-writing microfluidic devices. In this work the working of a single valve was demonstrated by printing another elastomeric channel (Fig.3.A.), known as the control channel, of the same material conformally over the already printed channel where the flow needs to be controlled. The control channel is pressurised with air, which causes the roof of the flow channel, which acts as the interface between both channels, to be deformed. This deformation decreases the channel's hydraulic diameter to zero causing the flow to stop (Fig.3.B.). The overlapping region was encapsulated by a layer of UV curable resin to not let the air pressure cause the control channel to expand upwards. This ensures none of the actuation pressure applied is lost in straining the control channel or causing it to burst due to the high pressures.

The control channels were interfaced with needles and connected to an external air supply for its actuation. These control channels were only conformally printed over a single channel forming single valves at the desired locations. These valves were found to require an actuation pressure of 150-300 kPa for flow pressures up to 30 kPa. The series of three valves were also combined serially to create a peristaltic pump by using a three-phase peristaltic code to programme the pneumatic supply. A multiplexed flow system where a single control channel actuates multiple valves was not demonstrated.

2.4. Physics of Microfluidic Flow

In the microscale regime, the flow tends to be laminar[44] because of the small channel cross-sections and low volumetric flow rates that are allowable.[45] In some cases, the laminar flow property poses challenges in applications like mixing, as diffusion becomes dominant at this scale.[46] The difficulties encountered in mixing are particularly relevant in biological applications. As a response to these challenges, there have been several advancements in the field.[47,48,49] On the other hand, the laminar flow characteristics in the microscale regime allow innovations such as the "Quake-style" valve, which can be explained by analysing the Navier-Stokes equations that govern fluid flow.

The Hagen–Poiseuille Law serves as a valuable approximation for understanding a pressure-driven flow in the laminar regime within a circular pipe.[50] This analytical solution is derived from the Navier-Stokes equation, relying on assumptions such as laminar, viscous, and incompressible flow.[51] To understand the working of the microfluidic valve in this work, employing computational fluid dynamics (CFD) can be a resource-intensive and time-consuming process.[52] The Hagen–Poiseuille law offers a simpler approach to understanding the working of the valve. Analogous to Ohm's law,[53] this law draws parallels between a pressure drop in a fluidic network to a voltage drop[54] in an electric circuit. This analogy provides a simple approach to comprehend the valve's operation in stopping the flow where the overlapping region of the control channel

functions as a resistor, increasing the resistance of the flow and consequently bringing down the flow rate to zero.

$$\nabla \cdot v = 0 \tag{1}$$

$$\frac{\partial v}{\partial t} + (v \cdot \nabla)v = -\frac{1}{\rho}\nabla p + \nu\nabla^2 2v \tag{2}$$

Eqn. (1) and (2) represent the mass and momentum conservation equations that for the Navier Stokes equations. Considering a steady, incompressible Newtonian flow in a circular pipe, an analytical solution for the volumetric flow rate, Q, can be derived by solving equations (1) and (2) which is presented in equation (3). Comparing the expression for the flowrate in equation (3) to Ohm's law, the resistance of the flow is given in Eqn. (4)

$$Q = \frac{\pi r^4 \Delta P}{8\eta L} \tag{3}$$

Where, Q is the volumetric flow rate, r is the radius of the pipe, ΔP is the pressure drop, η is the viscosity of the fluid, and L is the length of the pipe.

$$R = \frac{8\eta L}{\pi r^4} \tag{4}$$

In direct-ink-writing microfluidics, the flow channels are printed with a triangular cross section and not a circular one for ease of printing. An estimation of the cross section can

be approximated with the help of a geometric constant, hydraulic radius, which is given $\frac{2A}{P}$, where A is the cross-sectional area and P is the wetted perimeter of the flow.

$$R_h = \frac{8\eta L}{\pi(\frac{2A}{p})^4} \tag{5}$$

Therefore, from equation (5), the flow resistance is maximum as the cross-sectional area approaches zero as they are inversely proportional. The wetted perimeter includes the portions of the channel walls in contact with the fluid, which means that even as A approaches zero, the wetted perimeter is still non-zero. The above hypothesis can help conclude that the flow resistance is directly proportional to the length of the constriction to the flow and inversely proportional to the cross-sectional area of the channel.

2.5. Quake Valve Multiplexing

The membrane valve was adapted to create high-density microfluidic chips that contained hundreds of valves on a single chip. While designing a macroscale device consisting of multiple channels of flow, it is necessary to keep the number of inputs for control to a minimum. This optimization will reduce the complexity of the device and reduce the amount and cost of peripheral equipment required for the functionalization of these devices. To achieve this in microfluidic devices fabricated by soft lithography, a method was introduced to utilize combinatorial arrays of binary valve patterns to minimize the

number of control inputs. This requires a single control channel to overlap multiple flow channels whilst actuating only half of them, leaving the other half to remain open.

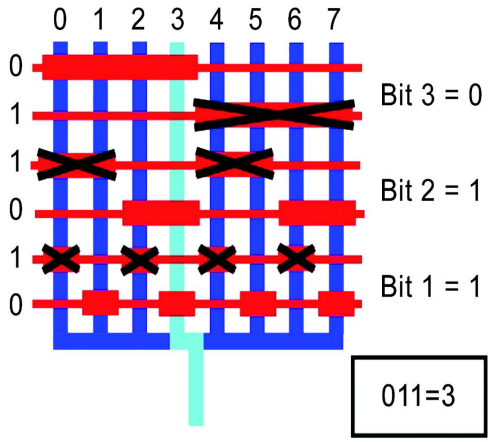

Figure 4. Working of multiplexed microfluidic devices[5]

As seen in Fig.4., the blue lines represent the flow channels, and the red lines represent the control channels. The point of overlap between both these lines forms a valve. The actuation pressure is chosen such that only the control channel sections with a wider overlap cause the membrane to deflect. Fluidic multiplexing allows large-scale integration of microfluidic devices by control of 2 $\log_2$ n flow channels with only n control channels. To not turn off the flow in the channels where it is not required to, the width of the control channels was reduced at the specific overlaps. Reducing the width of the control channels increased the pressure required for activating the valves, leading to the flow under those reduced-size overlaps to not being stopped.

2.6. Microfluidics For Biofilm Studies

Biofilms are multicellular aggregates of bacterial cells that are connected by a self-produced extracellular matrix and form under conditions where bacterial cells adhere to surfaces.[55,56] Biofilm research under ideal conditions does not allow consideration of real-time factors that affect their growth, such as the gradient of nutrients available.[57] or the effects of shearing forces in the environment.[58] Microfluidics offer unique opportunities to control environmental conditions at scales important for biofilm formation.[59, 60] They also allow us to observe how bacteria respond quickly to external changes.

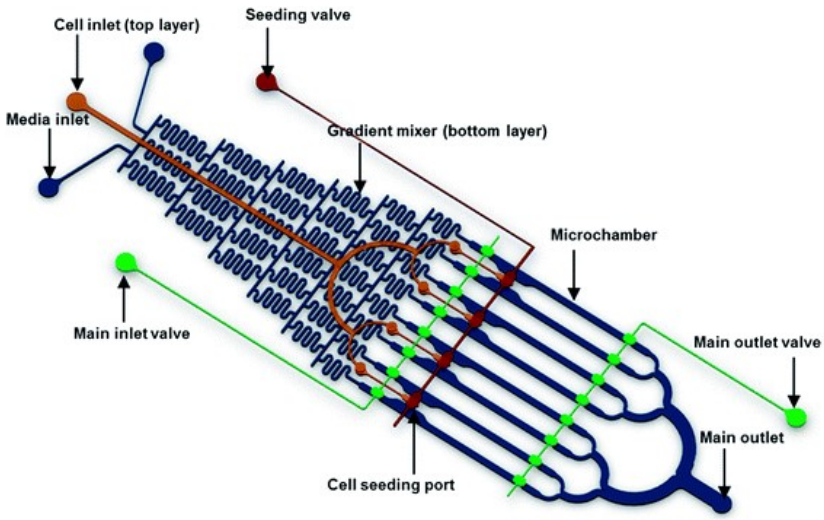

Figure 5. High throughput microfluidic device for biofilm studies[63]

Plasma-activated water (PAW) has evolved as a purifier on food surfaces and has been used in medical applications such as wound healing.[61] PAW contains reactive oxygen and nitrogen species (RONS), which have shown proof of concept for bacteria

inactivation.[62] Therefore, there is a need for microfluidic devices to study the effect of PAW on bacterial biofilms. Fig.5. shows a high throughput microfluidic device for studying biofilm response to different concentrations of soluble signals.[63] This design was adapted to design and fabricate by direct-ink-writing, a large-scale integrated microfluidic device for studying the effect of different concentrations of PAW on biofilms formed by PA14 strains.

CHAPTER 3

CONDUCTED RESEARCH

3.1 Printing Speed Optimization

The McAlpine research group successfully demonstrated the direct-ink-writing of single microfluidic channels, valves, and mixers on both planar and curvilinear substrates. RTV silicone was extruded through a 32 GA steel nozzle with a 0.1 mm inner diameter and onto a glass substrate. A source pressure of 25 psi, amplified seven-fold to 175 psi, facilitated the printing process at a speed of 1.0 mm/s, and the nozzle was maintained at a distance of 0.1 mm, as shown in Fig.6.A. While these parameters were suitable for proof-of-concept demonstrations, they are impractical for large-scale integrated microfluidic devices due to extended printing times and the nature of the material to cure due to moisture in the atmosphere.

For example, consider a microfluidic device 3D printed onto a 75 mm × 50 mm substrate with 16 flow channels (300 μm base width) and 8 control channels (0.8 mm base width). The estimated printing time based on the above printing parameters is around 12 hours, which is not feasible. This is because, RTV Silicone cures over time, leading to changes in rheological properties that hinder extrusion during prolonged printing periods. Fig.6.B.

shows the increase in the storage modulus of RTV silicone over time, indicating the curing of the material in ambient conditions.[21] It also contradicts the goal for direct-ink-writing to be a method for rapid prototyping microfluidic devices. Thus, a methodology was needed to enhance the printing speed of RTV silicone for the realization of large-scale integrated microfluidic devices.

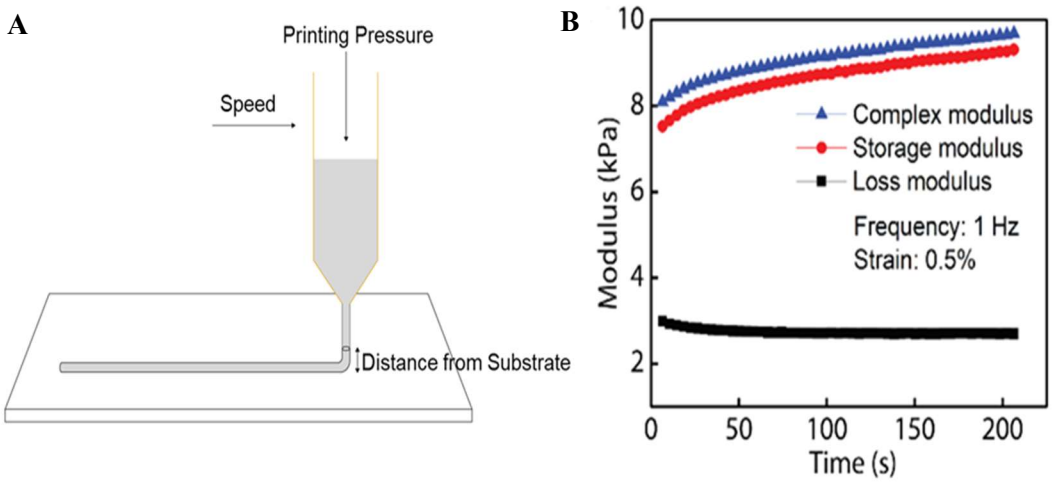

Figure 6. Direct-ink-writing of RTV silicone (A) Illustration of direct-ink writing parameters (B) Increase in RTV silicone storage modulus over time[21]

3.1.1. Studying the Effect of Varying Printing Parameters

First, silicone lines were extruded and printed onto a glass substrate to investigate the impact of different printing parameters on the dimensions of the extruded silicone filaments. The qualitative insights gained from this study were utilized to develop an algorithm aimed at optimizing the printing process for microfluidic devices. The

experiment employed a 32 GA nozzle, which is consistent with the work of the McAlpine research group in their demonstration of direct-ink-writing microfluidic devices. The nozzle was positioned at 0.1 mm from the substrate, matching the internal diameter of the nozzle as per the recommended protocol to minimize silicone swelling.[33] Source pressures ranged from 25.0 psi to 35.0 psi in increments of 2.5 psi and amplified seven-fold, while printing speeds varied from 1.0 mm/s to 3.0 mm/s in 0.5 mm/s increments. Filament profiles were subsequently examined using a surface profiler equipped with a high-precision force sensor to analyze variations in their dimensions.

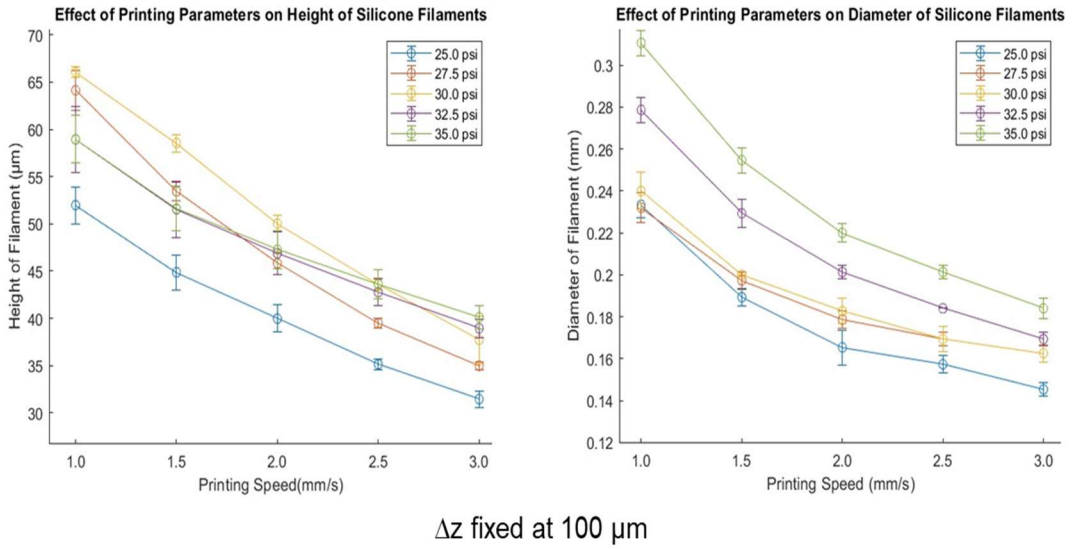

Figure 7. Effect of printing parameters on dimensions of silicone filaments (N = 9)

Fig.7. illustrates the variation in dimensions of the extruded silicone filament based on printing parameters. Both filament diameter and height increased when source pressures were raised from 25.0 psi to 35.0 psi. However, an important observation was that, at all tested pressures, consistently increasing the printing speed resulted in dimension reduction. For instance, from the graph in Fig.7., a filament with a diameter of 0.22±0.02 mm could be printed at all tested pressures by simply varying the speed from 1.0 mm/s to 2.0 mm/s. This trend also applies to filament heights. Therefore, this study shows that as long as the source pressure can be increased to a safe and allowable limit, the change in the filament dimensions can be compensated for by increasing the speed as required. This insight formed the basis for developing an algorithm to optimize the printing speeds of 3D printed microfluidic devices.

3.1.2. 3D Printing Optimization Methodology

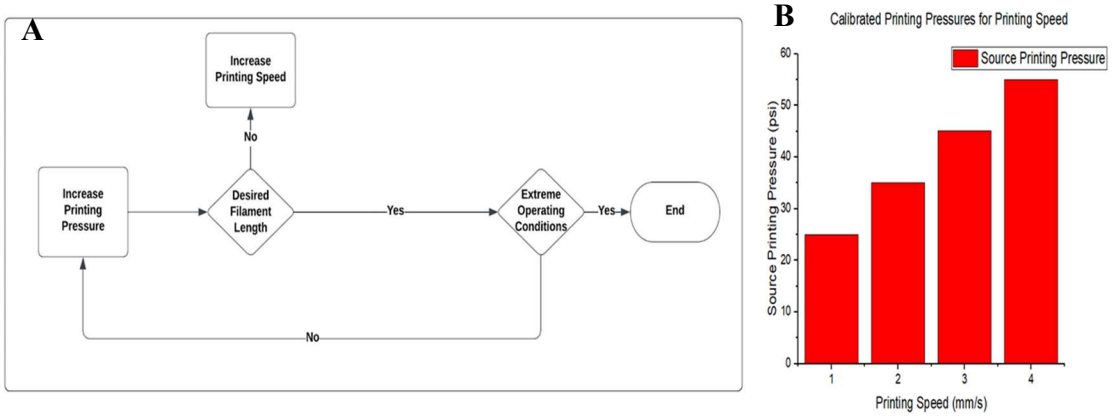

Figure 8. 3D printing optimization (A) Methodology to increase printing speed (B) Calibrated printing pressures for different printing speed.

The methodology depicted in Fig.8.A. aims to optimize the printing speed for large-scale integrated microfluidic devices. The source pressure for ink extrusion is gradually increased, and triangular microfluidic channels with a base width of 400 μm are 3D printed at varying speeds until all layers are optimally printed. This process is repeated until the source pressure reaches 55 psi. The printing speed is then adjusted until optimal channel printing is achieved at 4 mm/s, four times the initial speed as indicated in Fig.8.B.

The final printing pressure is seven times the source pressure, resulting in a final pressure of 385 psi. Notably, this pressure exceeds 50% of the limit of the mechanical pressure amplifier and the maximum pressure limit of the source. To optimally print channels at this pressure, the speed is further increased and is found to be 4 mm/s. Consequently, the printing speed of the flow channels is improved up to 4 times the initial speed envisioned in the conceptualization phase. This methodology demonstrates a systematic approach to achieving significant enhancements in the printing speed of microfluidic devices through careful adjustment of source pressure for extrusion and printing speed.

3.1.3. Optimizing the Printing Speed of Control Channels

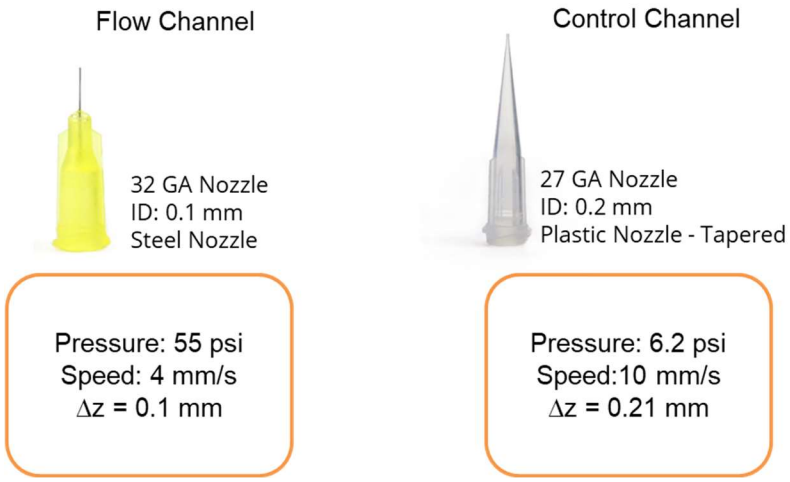

Figure 9. Comparison of nozzles for printing speed optimization

The control channels, with a base width exceeding 800 µm and approaching the millimeter range, require extended printing times due to their larger dimensions and the need for conformal layering. This longer printing time is a consequence of requiring more layers than flow channels and the need to be conformally printed over them. The printing speed of these channels is the major bottleneck for production as they take more than double the printing time required for flow channels. Hence, an even more optimal method for 3D printing control channels was a necessity. The solution involved replacing the 32GA steel nozzle with a 27GA tapered plastic nozzle, as illustrated in Fig.9.

Fig.9. compares the calibrated printing parameters of the 32GA nozzle and the 27GA nozzle. The yellow nozzles, with a smaller inner diameter and precision owing to their steel composition, provide superior resolution. In contrast, the clear plastic nozzle has twice the inner diameter, allowing control channels to be printed with half the number of layers compared to the yellow nozzle. The tapered design, according to Bernoulli's principle, creates a pressure gradient, enabling significantly lower printing pressures. Plastic, being less rigid, also causes less constriction to the flow compared to steel and reduces extrusion pressure, overcoming limitations present with the yellow nozzle. These improvements enable printing speeds of 10 mm/s at source pressures as low as 6.2 psi.

Given that control channels do not demand the same level of precision and resolution as flow channels due to their wider base widths, the entire process can be optimized with the help of clear nozzles. As a result, control channels can be printed 20 times faster than the existing method, demonstrating a substantial enhancement in printing time.

3.2. Valve Characterization

The first step to achieve large-scale integration is to demonstrate the 3D printing of control channels over multiple flow channels. The existing valve design was adapted and modified for accurate layering of conformal channels over multiple flow channels. For this, the movement of the nozzle was accurately calculated over isosceles triangle cross-

sectioned flow channels with an angle of 45°. This calculation was based on the diameter of the nozzle and the height at which it needs to be maintained from the target surface for conformal direct-ink-writing.

The toolpath calculation was employed to demonstrate an array of four valves. A device with four individual channels of base widths 200 μm and 400 μm was 3D printed on a glass substrate, as depicted in Fig.10.A. Control channels of widths 0.8 mm, 0.9 mm, and 1.0 mm were successfully printed over the flow channels to form valve arrays and encapsulated with UV resin. These valves were then connected with 25 GA steel tubes to a piezometric valve system linked to a source of air pressure, as shown in Fig.10.B. A pressure-driven flow was generated and connected to the microfluidic flow channels. The flow from these channels was connected to a flow rate sensor to measure the flow rate and identify the actuation pressure variation for different dimensions of the control channel.

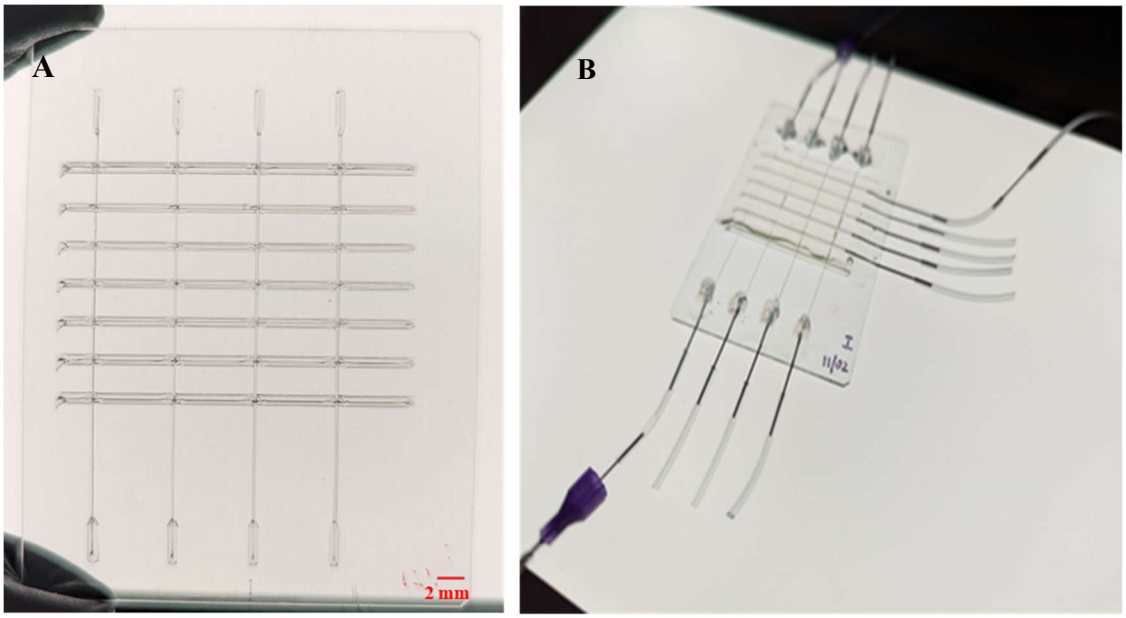

Figure 10. 3D printed device for valve testing (A) Control channel overlapping multiple flow channels (B) Device interfaced with steel tubing for connections.

The pressure control system ramped up the actuation pressure of the valve supplied from the source at a user-defined rate. Simultaneously, the flow rate was measured as a response to the control channel being closed by the actuation pressure. The pressure at which the valve starts to close is defined as the actuation pressure as the flow rate drops exponentially due to the decrease in cross-sectional area. For the flow channels of base width 200 µm and height 200 µm, the source pressure was set at 180 mbar for the 200 µm channel and 175 mbar for the 500 µm channel to induce a flow rate of approximately 13 µl/min. The single valve tested by the McAlpine research group showed [21] an increase in actuation pressure required to close the microfluidic channel as the pressure of the flow was increased. In this work, the effect of changing dimensions of control

channels and flow channels was tested to verify the data against the principle of the Hagen-Poiseuille flow, and the actuation pressure range for the valves was determined.

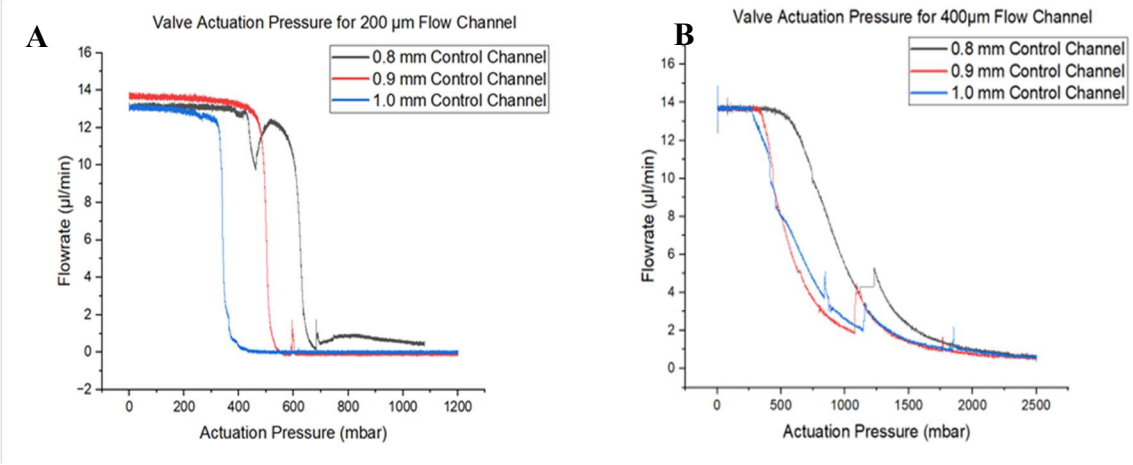

Figure 11. Valve actuation pressure for (A) 200 µm flow channel (B) 400 µm flow channel

The actuation pressure range for the valves was determined by testing the effect of changing the dimensions of control channels and flow channels. First, the 200 µm channel (Fig.11.A.) was closed with control channels varying from 0.8 to 1.0 mm. The actuation pressure was ramped up from 0 mbar to 1200 mbar within 440 seconds. The actuation pressure required to close the valve decreased from nearly 600 mbar to 350 mbar by increasing the width of the control channel by 200 µm. This decrease aligns with the Hagen–Poiseuille Law, where flow resistance increases with the length of the resistor. Similar results were obtained for a 400µm channel (Fig.11.B.) where the actuation pressure was ramped up to 2500 mbar in 440s. In this experiment, the point of closing

was found to be at an actuation pressure between 400 mbar to 650 mbar, showing a trend of increasing actuation pressure required for larger widths of the flow channel despite not exhibiting a pronounced increase in flow resistance as explained by the flow rate of a circular flow channel being directly proportional to the fourth power of its radius. This can be explained by the factor of error induced by making the hydraulic radius approximation.

3.3. Reinforcement Layer

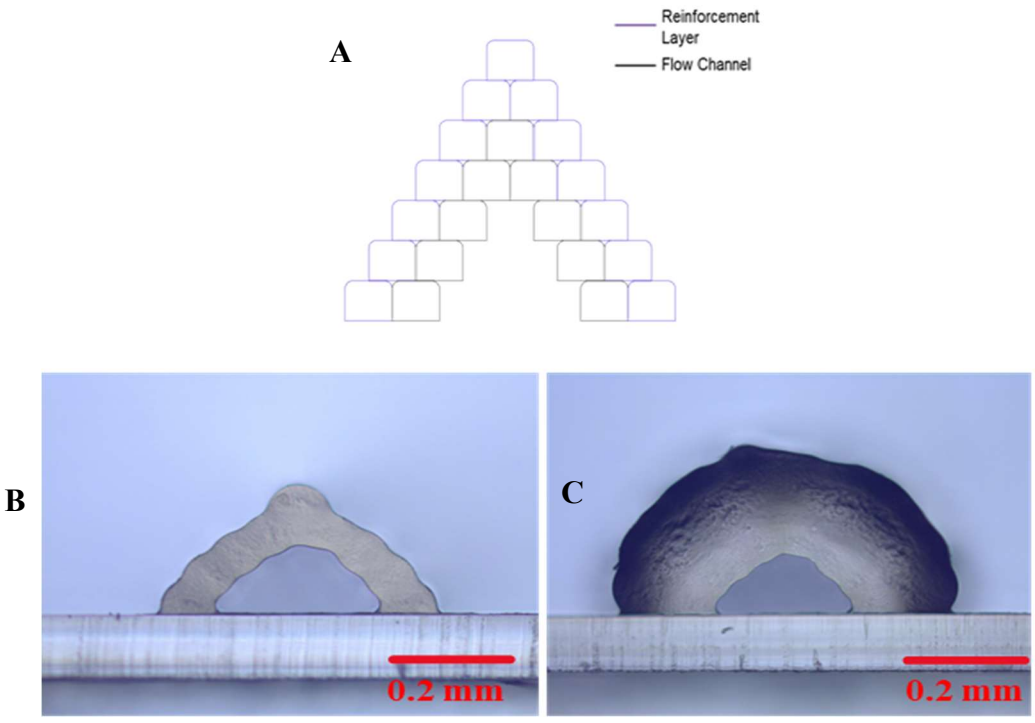

Figure 12. Reinforcement layer (RL) over a flow channel (A) 3D printing methodology (B) flow channel cross-section with RL (C) Flow channel cross-section without RL

To achieve multiplexed flow using a network of control channels laid over flow channels, it is necessary that some control channels do not close certain valves even when they are pressured with air. In large-scale integration of microfluidic devices fabricated by soft lithography, this is achieved by reducing the width of the control channels at points of overlap where the valve needs to stay open even during actuation. With the existing method of direct-ink-writing control channels, constantly changing the width of control channels is a challenge as the constant change in dimensions can lead to an increase in the probability of defective channels and increase the lead time from design to fabrication due to its complexity. This challenge is avoided by printing silicone filaments between the interstitial spaces of the flow channel layers (Fig.12.A) at localized sites where the valve should not be closed under the overlapping intersection. The reinforcement layer (RL) effectively achieves this by increasing the thickness (Fig.12.B and Fig.12.C.) of the flow channel, resulting in a higher actuation pressure required to deflect the membrane.

For 3D printing the reinforcement layer, the printing parameters were maintained the same as the printing of flow channels. This uniformity in printing parameters allows for a consistent method of increasing thickness, and consequently, printing a control channel over a reinforcement layer requires the same toolpath calculation as printing them over flow channels. Therefore, the reinforcement layer was printed with a source pressure of 55 psi amplified to 385 psi with a printing speed of 4 mm/s. A single layer of reinforcement increases the outer dimensions of the flow channel by a factor of 0.2 mm

in width and 0.1 mm in height. This uniform increase allows simple algorithms for producing G-code for control channels.

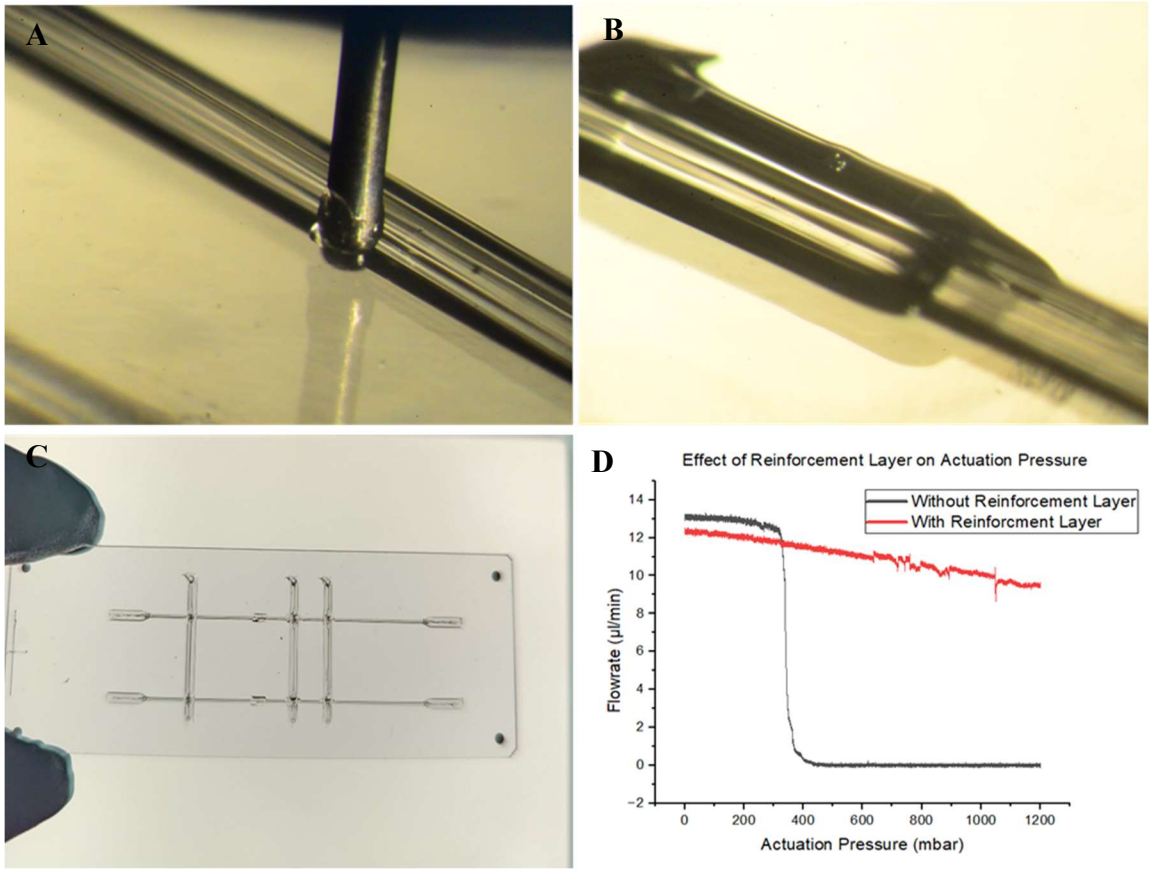

Figure 13. 3D printing and testing of reinforcement layer (RL) (A) Flow channel without RL (B) Flow channel with RL (C) Device for testing flow channel with RL (D) Effect of RL on actuation pressure

This concept is demonstrated in Fig.13., showing the roof of the flow channel before (Fig.13.A.) and after (Fig.13.B.) printing the reinforcement layer. The working of the reinforcement layer was tested with control channels of 1.0 mm width, which were

printed over 200 µm wide flow channels both with and without a layer of reinforcement (Fig.13.C.) and encapsulated with UV curable resin. A flow rate of 13 µl/min was set through these pipes by pressurizing a fluid source by 175 - 180 mbar. Once the flow reached a steady state, the control channels with a width of 1.0 mm were ramped up with an air pressure of 1200 mbar. The graph in Fig.13.D. shows the response to the actuation pressure for the flow rate under both conditions. With similar channel dimensions and actuation pressure, the flow does not completely stop with the control channel that is laid over a reinforcement layer. This serves as a proof of concept, confirming the effectiveness of using a layer of reinforcement in preventing the closing of flow channels overlapped by a control channel.

3.4. High Burst Pressure Silicone Microfluidic Channels with Fillers

The channels printed with RTV Silicone do not have sufficient mechanical strength to withstand the high pressures for valve actuation. This led to the development of these channels being encapsulated with a layer of UV-curable resin to withstand much higher pressures and function as a valve. The resin encapsulation adds a different form factor to the device by allowing channels to be actuated with very high pressures for valve functioning. This section explores a method to eliminate the encapsulation step from the fabrication process by improving the mechanical strength through the introduction of fillers in the material. There are two factors that contribute towards high burst pressures and form factors:

- The mechanical strength of the material to withstand large deflections, and
- Its adhesion to the substrate to prevent channel detachment.

Improving these two factors can potentially eradicate the need for an encapsulating procedure, leading to complete automation of the fabrication process.

For the additives to be viable for use for direct-ink-writing of microfluidic devices, they need to satisfy the following criteria:

- Size of the additive smaller than the nozzle's inner diameter,
- Low density to prevent collapse due to own weight, and
- Low yield stress for extrusion to be viable.

As the density needs to be low, large volumes can prevent polymerization between the layers of silicone, leading to poor adhesion. Two additives were identified that fit the criteria: Glass microspheres size < 100 μm and UV resin used for encapsulation. The concept of fabricating a valve using these additives in silicone was explored.

The next step was to test whether these additives improve the mechanical properties of silicone. The ink was prepared by adding the percent by weight of the additives with the silicone as the solvent. The mix was then placed in a high-speed mixer for 2 minutes at 2000 rpm and then a further 2 minutes at 2200 RPM. Once the ink was formulated, it was loaded into the syringe for extrusion. Rectangular patches with dimensions 36 mm × 4

mm × 0.8 mm were printed to test how much the mechanical properties of the material could be improved with the help of additives. The printing lines for these patches were parallel to the direction of tensile testing. The patches, post-curing, were clamped from both ends for uniaxial tensile testing to determine the improvements in mechanical properties. The young's modulus calculated from the stress-strain curves obtained from the tensile testing of the rectangular patches. Fig.13.A. shows an increase from 157 kPa to 474 kPa for adding 10 wt.% of UV glue and 562 kPa for adding 10 wt.% of glass microspheres. This established a possibility for the 3D-printed channels with additives to have good potential for removing the encapsulation layer.

After tensile testing, the materials were used at different concentrations to test the printability. The printing source pressure for a speed of 2 mm/s was calibrated based on the set protocol. Silicone filaments were extruded through a 27 GA nozzle at 0.2 mm from the substrate. The printing pressure was set to that of RTV silicone and increased until the channels of width 800 μm were printed seamlessly with individual filament widths of 200 μm. The printing pressures of the different inks that were developed are mentioned in the table in Fig.14.

Material	Source Pressure for Extrusion at 2mm/s Printing Speed (psi)
RTV Silicone	3.2
RTV Silicone + 10 wt.% UV Resin	10.2
RTV Silicone + 10 wt.% Glass Microspheres	5.2
RTV Silicone + 10 wt.% UV Resin + 1 wt.% Glass Microspheres	8.4
RTV Silicone + 10 wt.% UV Resin + 7 wt.% Glass Microspheres	13.0

Figure 14. Table for calibrated source pressures for extruding silicone with fillers.

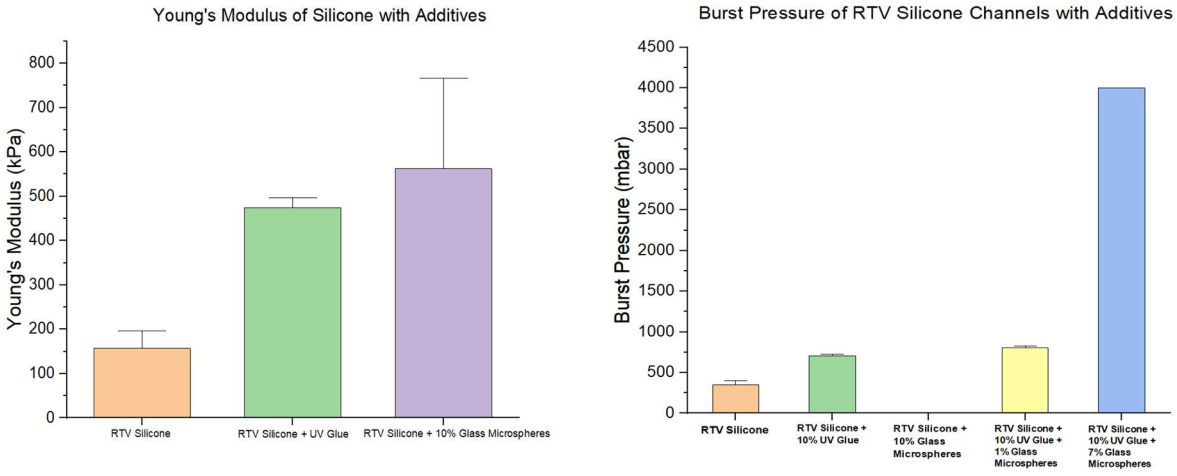

Figure 15. Enhancement of silicone with fillers (A) Young's modulus of silicone with fillers (N = 6) (B) Burst pressure of microchannels made of silicone with fillers (N = 6)

After printing channels with a thickness of 200 µm, burst pressure was assessed by pressurizing the channels with air. One end of the channel was sealed, and the open end was connected to an air pressure source, increasing by 25 mbar at 10-second intervals. This intermittent pressure allows for the identification of the point at which the channel bursts. The source pressure was incrementally raised up to 4000 mbar. Fig 15.B. illustrates the increase in burst pressure for channels with different concentrations of fillers.

As depicted in Fig.15.B., channels made of RTV silicone consistently burst at pressures ranging from 325 mbar to 400 mbar. This slightly increased to 700 mbar for channels printed with 10 wt.% of UV glue. However, channels printed with silicone containing 10 wt.% of glass microspheres could not withstand any air pressure due to the high volume of particles that led to poor adhesion of the microchannels to the substrate.

To enhance adhesion, various concentrations of glass microspheres were added to a mixture of RTV silicone and 10 wt.% of UV Glue. Adding 1 wt.% of glass microspheres to this mix improved burst pressures to 800 mbar. The concentration of glass microspheres was increased up to 7 wt.%, beyond which the printability was affected. At this composition, the channels were capable of withstanding pressures up to 4000 mbar without bursting, and the process could be repeated even after pressure removal.

Despite successfully increasing burst pressure beyond the actuation of these valves, it did not function as expected when control channels were printed with RTV silicone containing 10 wt.% UV glue and 7 wt.% glass microspheres. This is attributed to the insufficient stiffness of the material to function as a valve, as burst pressure alone is not the limiting factor. The channel should be stiff enough to direct all the energy supplied by the actuation pressure toward membrane deflection without wasting it by deflecting the roof of the control channel. Therefore, developing a methodology to print multiple layers of the control channel could further enhance mechanical properties and unlock the potential of this method for fully automating the 3D printing of large-scale integrated microfluidic devices.

3.5. Demonstrations of Large-Scale Integrated Microfluidic Devices

3.5.1. 2×2 Multiplexer

Figure 16. 2×2 Multiplexer (A) 3D printed device (B) Microscopic image of RL.

A 2×2 multiplexer was designed and fabricated, as shown in Fig.16.A., to function as a proof of concept for the development of a large-scale integrated device. The device features two input flows converging to a single output. Two control channels are printed over both the inlets. However, a reinforcement layer is strategically placed for one of the inlets beneath both control channels (Fig.16.B.). This allows each control channel to close only one inlet even though they are placed over both. The inlets were designed with a width of 300 μm, while the control channels were 900 μm wide. A layer of UV-curable resin was used to encapsulate the control channels, and the entire structure was cured using 405 nm UV light.

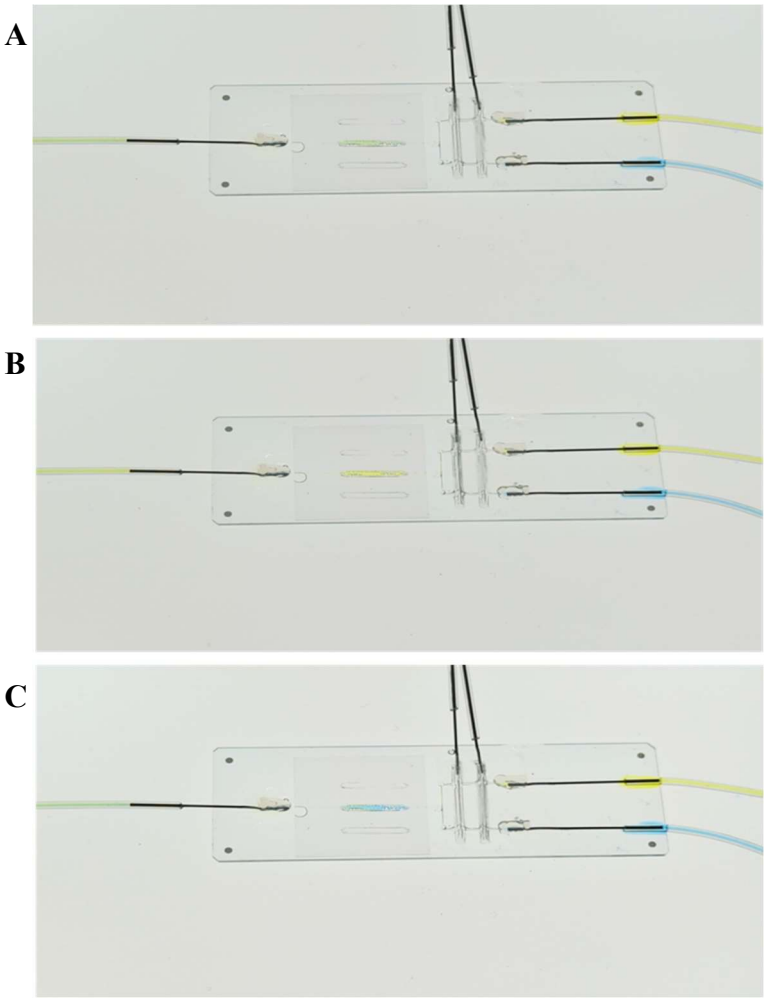

Figure 17. Working of 2×2 multiplexer (A) Control channels not actuated (B, C) Single control channel actuated.

To visually demonstrate the working mechanism, both inlets were connected to distilled water mixed with blue and yellow food dyes. The design incorporated a viewing window (Fig.16.A.) to improve imaging of the multiplexer's operation. Initially, with neither control channel actuated, the flow in the viewing window displayed a mixture of both yellow and blue flows (Fig.17.A.). However, when the control channels were individually pressurized to 1500 mbar, the flows in both inlets were controlled independently,

resulting in the viewing window turning yellow (Fig.17.B.) and blue (Fig.17.C.), respectively.

This demonstration successfully validated the concept of using a reinforcement layer to create multiplexed devices for microfluidic applications. The scalability of this concept will pave the way for large-scale integrated microfluidic devices fabricated by direct-ink-writing.

3.5.2. 16×8 Multiplexer

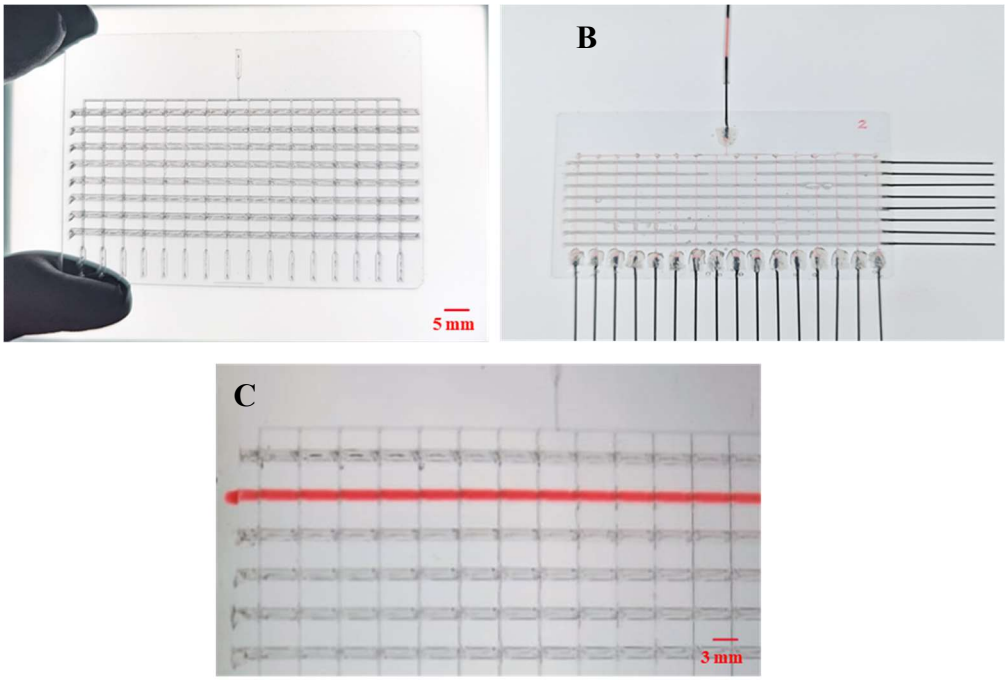

Figure 18. 16×8 multiplexer (A) 3D printed 16×8 multiplexer (B) Working of flow channels of the multiplexer (C) Seamless printing of control channel over 16 flow channels.

A 16×8 multiplexer was designed to demonstrate the printability of large-scale multiplexed microfluidic devices. Leveraging the multiplexing principle, this design only required 8 control channels with a width of 0.9 mm to control 16 flows that diverge from a single input. The final 3D printed device depicted in Fig.18.A. includes 64 reinforcement layers, enabling the multiplexing of the device. The network, printed on a 75 mm × 50 mm substrate, comprises an array of 128 valves, representing the highest density achieved for a microfluidic device using this method.

Optimizing the printing speed, as discussed in earlier sections, enabled the successful printing of this device. The printing time was significantly reduced from ~12 hours to less than 1.5 hours, demonstrating the feasibility of printing such a large-scale device using this method. Fluid was passed through the flow channels (Fig.18.B.), illustrating the seamless printing of the flow network. Distilled water mixed with red dye (Fig.18.C.) was also passed through the control channel, overlapping 16 different flow channels without any leaks, showcasing the seamless printing of the highest number of overlaps achieved using direct-ink-writing. Each of these control channels was printed in approximately 2.5 minutes, a notable improvement compared to the estimated ~50 minutes required with the earlier methodology.

The working demonstration of the multiplexor could not be completed due to various errors in fabrication which include:

- Defects in the flow channel,
- Perfect functioning of all 128 valves and 64 reinforcement layers, and
- Uneven distribution of UV resin that forms the encapsulation.

3.6. Applications of Automated Microfluidic Devices

The above principles were used to design and fabricate microfluidic devices for two applications: 1. A lab-on-a-chip device for studying the effect of plasma-activated water on bacterial biofilms under flow conditions, and 2. A multiplexed microfluidic dispenser for functionalizing a graphene bio-sensor for disease detection. This section discusses in detail, the design developed for these devices based on inputs from different collaborators for large-scale integrated microfluidic devices. The devices were successfully conceptualized, and 3D printed by extending the direct-ink-writing of self-supporting structures developed by the McAlpine Research Group.

3.6.1. Lab-on-a-chip for Biofilm Studies

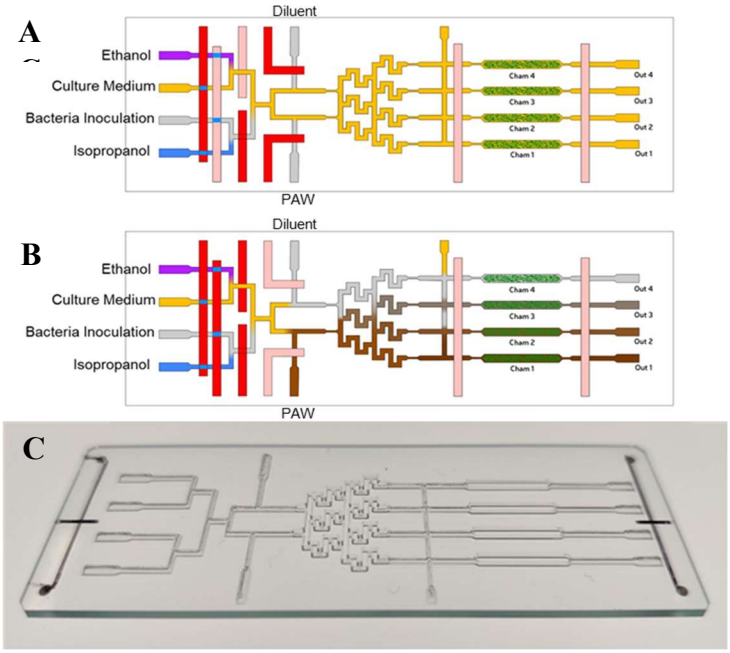

Figure 19. Lab-on-a-chip (LOC) for biofilm studies (A) Growing biofilm in device (B) Treating biofilm with different concentrations of PAW (C) 3D Printed LOC Device

A 3D-printed lab-on-a-chip (LOC) microfluidic platform was created for cultivating *Pseudomonas aeruginosa* (PA14) biofilm under dynamic flow conditions and evaluating its response to varying concentrations of plasma-activated water (PAW) for inhibiting or modifying bacterial growth. Fig.19.A. illustrates the design of the platform, which incorporates essential microfluidic components such as an input multiplexer, gradient generator, and culture chambers. The flow channels of the device were successfully 3D printed as shown in Fig.19.C.

The input multiplexer, depicted in Figure 19.A., includes 3D-printed microfluidic valves and reinforcement layers. This component allows the selection of different reagents, such as ethanol, bacterial culture, and culture medium, for delivery to the culture chamber where the bacterial biofilm grows. The gradient generator, shown in Figure 20.B., produces up to four different concentrations of plasma-activated water in the downstream culture chamber for testing the effect of the concentration of PAW on the grown biofilm. Multiple LOC devices can be operated simultaneously to assess the effectiveness of different species in plasma-activated water.

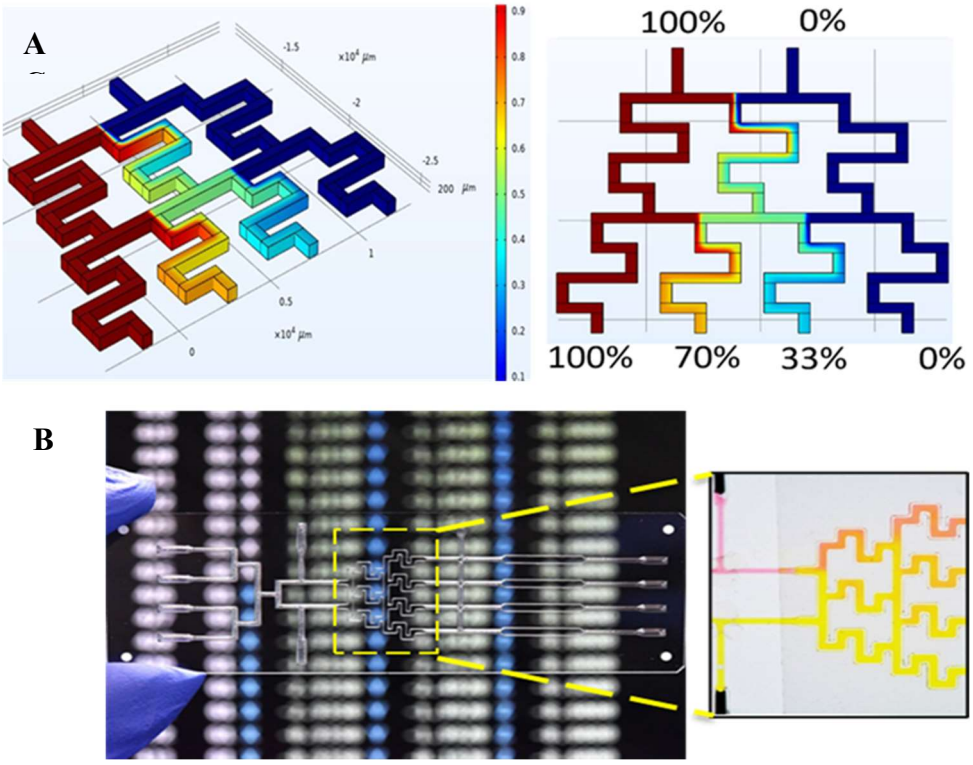

Figure 20. Gradient generator (A) COMSOL simulation of gradient generator (B) 3D printed LOC: working of gradient generator[Image Credit: Dr. Fujun Wang]

Fig.20. depicts the gradient generator designed to enhance mixing in the microfluidic device. It dilutes 100% of the concentration of plasma-activated water to multiple concentrations by mixing it with a diluent, such as saline solution. The design includes multiple 90° turns to induce dean vortices, promoting efficient mixing in the microscale. The concentration profile produced by the gradient generator was simulated on COMSOL Multiphysics, resulting in 100%, 70%, 33%, and 0% concentrations of PAW for testing PA14 biofilms.

Additionally, the LOC platform is adaptable for use with a microscope, enabling real-time analysis of biofilm growth and treatment. The culture chamber, shown in Figure 19.C., is created by stacking silicone filaments vertically to achieve a height of 0.5 mm, width of 1 mm, and length of 10 mm. A glass cover slip is carefully placed on top, creating a window for enhanced optical imaging compared to the triangular channels, where silicone filaments obstruct the view. This allows for fluorescent and brightfield microscopy of the biofilm in the device.

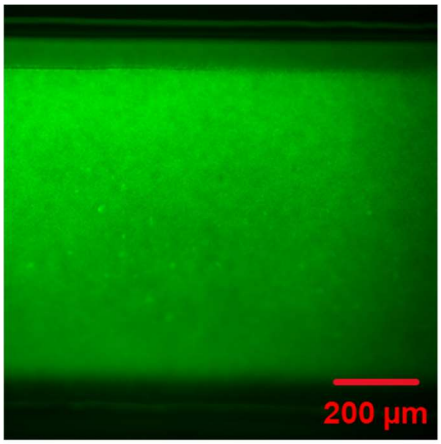

Figure 21. Fluorescent microscopy of Biofilm after 4 hours

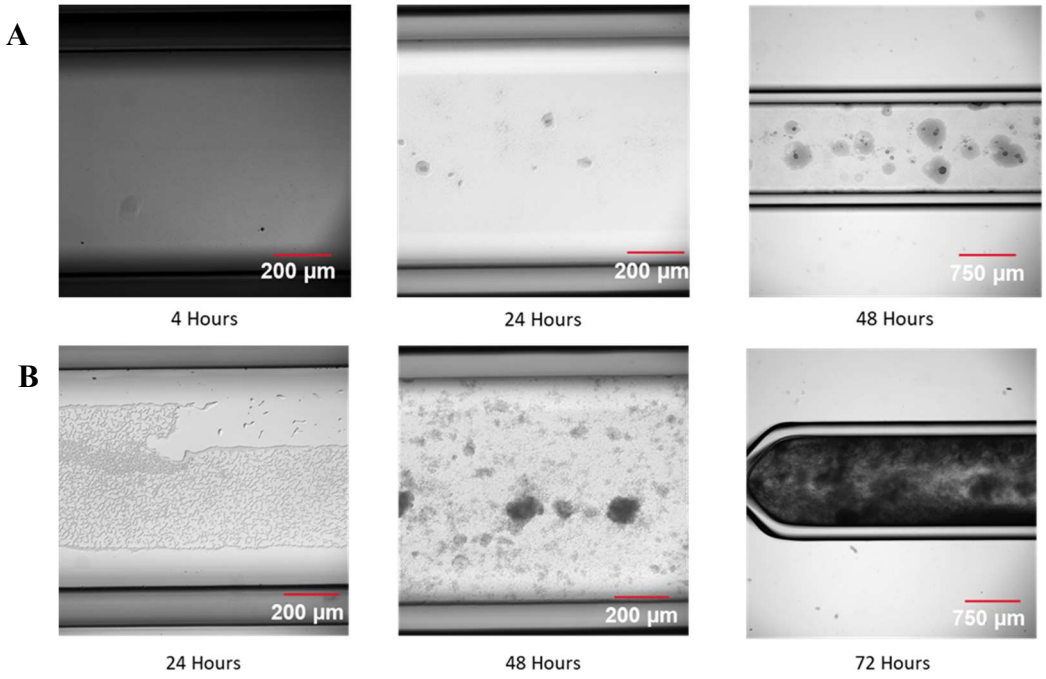

Figure 22. Growing PA14 Biofilm in Culture Chamber (A) 11µl/min flowrate (B) No-flow condition

Preliminary experiments were conducted to grow biofilm and image them in the 3D-printed culture chamber. The purpose of this preliminary experiment is to test the functionality of these microchambers for observing the formation of a *pseudomonas aeruginosa* biofilm in dynamic flow conditions. After sterilization of the chambers with ethanol and isopropanol, the channels were primed with LB broth as the culture medium and the liquid PA 14 culture was inoculated. Flow in the microchannel was paused for four hours to allow the seeded bacteria to settle on to the walls of the culture chamber as shown in Fig.21.

Observations were made under a 11µl/min flow of nutrient rich LB broth and non-flow conditions over 72 hours. Under flow conditions (Fig.22.A.), the biofilm microcolonies have a dense interior, due to the constant washing away of bacteria on the outer circumference of the microcolonies. These microcolonies could also be a feature of a constant supply of nutrients and the gradient of nutrients generated by the flow. In contrast, under non-flow conditions (Fig.22.B.), due to limited nutrient availability without a constant flow of the culture media, dense biofilm structures were formed as a survival instinct. Structural integrity issues were observed under flow conditions beyond 48 hours, with leakages at the interface between the silicone and the coverslip. However, these experiments established that the device was viable for growing bacterial biofilms and allowed high-resolution imaging for observing their development.

3.6.2. Microfluidic Multiplexer for Graphene Biosensor Functionalization:

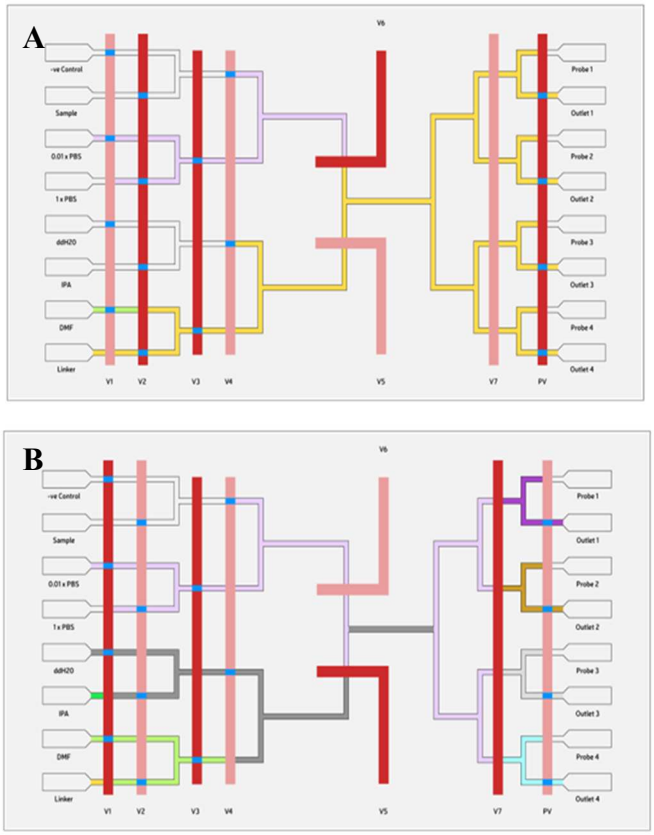

Figure 23. Design of multiplexed microfluidic dispenser for bio-sensor functionalization

The second application involved the design and fabrication of a microfluidic multiplexer for testing a point-of-care (POC) sensing device's functionality. The microfluidic multiplexer sequentially directs the flow of probe molecules, reagents, and analytes over a graphene sensor to facilitate the multiplexed diagnosis of various diseases on a single graphene chip (Fig.23.). This graphene-based biosensor comprises of four sensing regions (Fig.24.B), and the multiplexer automates the functionalization of these regions

to detect different diseases during the product development phase of the diagnostic device.

The microfluidic multiplexer consists of eight inlets, including those for linker molecules and dimethylformamide (DMF), which are essential for immobilizing probe molecules on the graphene sensor. To ensure proper functionalization, the sensors undergo a series of washing steps with isopropyl alcohol (IPA), ddH20, and a rinse with 1×PBS to eliminate unattached molecules. Despite having 8 inlets, the multiplexer is efficiently controlled by just 6 channels by employing multiplexing principles.

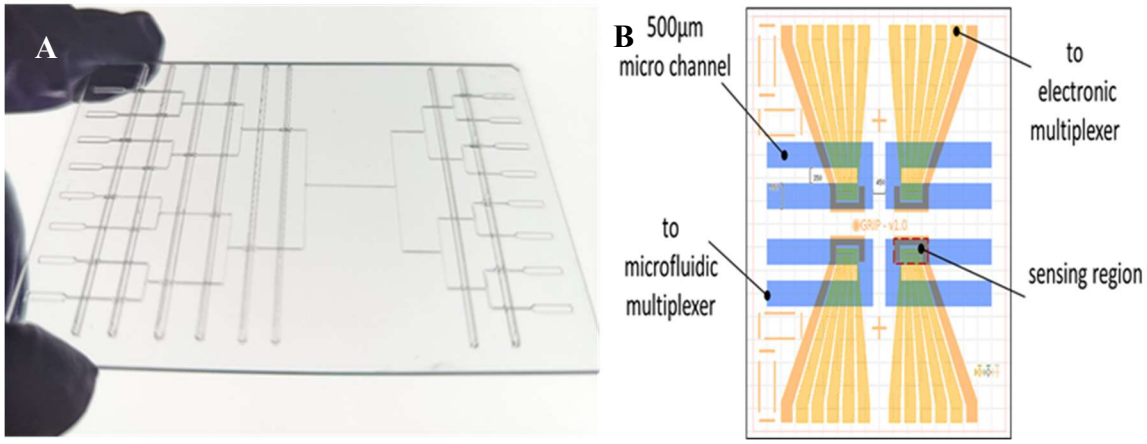

Figure 24. 3D Printed Multiplexed Microfluidic Dispenser (A) and (B) 3D Printed Channels on Bio-sensor.

The probe molecules, which are molecules that attach to the sensor to test for different diseases, are introduced through ports P1-P4, regulated by the probe valve, followed by additional washing steps with ddH20, 1×PBS, and 0.01×PBS to remove excess

molecules. All reagents and probe molecules converge at the four outlets, connecting to 3D-printed channels on the graphene biosensor. Once the functionalization process is complete, the multiplexer facilitates the flow of analytes, initiating the sensing process.

The multiplexer was successfully 3D printed (Fig.24.B.) according to the required design without any defects. The printing time was 40 minutes, achieving rapid prototyping and showcasing the efficiency of the optimized printing parameters.

CHAPTER 4

ADDITIONAL PROJECT DETAILS

4.1. Analyzing Surface Profile of Silicone Filaments

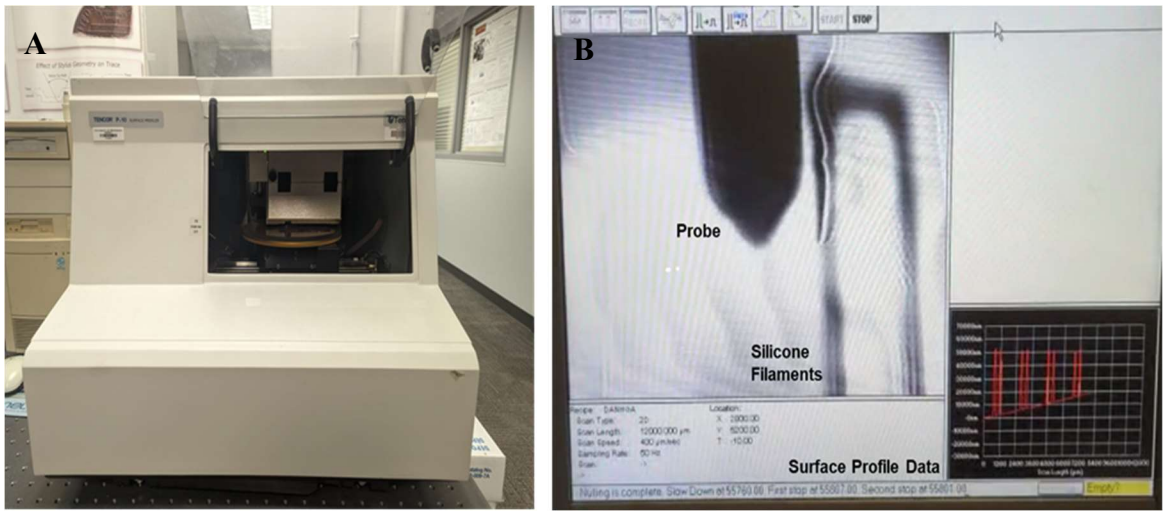

Figure 25. Analyzing the profile of extruded silicone filaments (A) Tencor P10 profilometer (B) User-Interface of the Tencor P10 Profilometer

The dimensions of the extruded silicone filaments at different speeds and source pressures were analyzed using the Tencor P10 Profilometer at the UMN characterization facility. 3D printed samples were positioned on the surface profiler stage, where a mechanical probe, which is a low-force micro head sensor, is moved along the substrate's length, capturing profiles of the silicone filaments. The probe has the ability to measure micro-roughness with up to 0.5 Å resolution. A MATLAB code was created to extract filament height by identifying peaks in the surface profile data, whereas filament

diameter was determined by analyzing points where data began to peak and returned to the surface level. This method facilitated precise measurement and analysis of the silicone filaments' characteristics.

4.2. Design to 3D Print Methodology

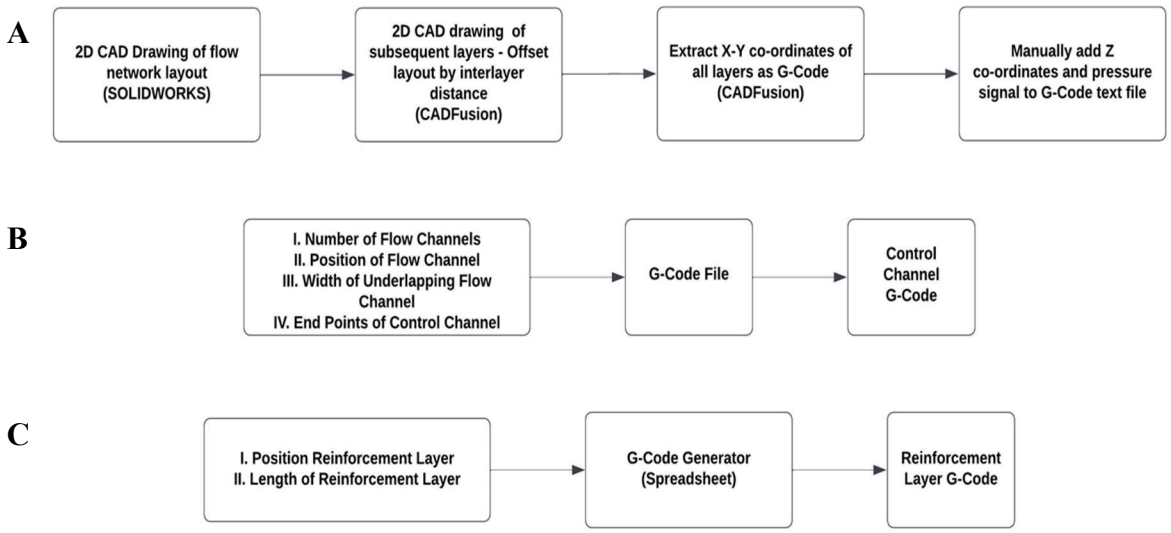

Figure 26. Design to 3D print methodology of (A) Flow channel network (B) Control channels (C) Reinforcement layers

Fig.26. illustrates the step-by-step methodology for developing various components of a 3D-printed large-scale integrated microfluidic device, starting from the initial design to G-Code generation. The network of flow channels is first drafted as a 2D CAD drawing in a CAD software (SOLIDWORKS) based on design requirements. The shape and dimensions of this drawing serve as the foundational layer for the 3D printed network. Subsequent layers are designed with an offset, converging at the top to form a triangular

cross-section. The CAM software utilizes the offset feature to generate coordinates for these layers, which are then incorporated into the G-Code. Manual editing of the G-Code involves adding Z coordinates for each layer and signals to the pressure control system to initiate and stop the extrusion of the material.

For the control channel, a default G-code file was created using the AEROBASIC Programming Language of the AEROTECH motion control system, which includes the format of the control channel G-Code. Users can input variables such as the number of overlapping flow channels, their positions, base widths, and endpoints, resulting in a customized G-code for 3D printing the control channel. Similarly, for the reinforcement layer, user input data, such as its position and length, is used to generate the G-code necessary for 3D printing a reinforcement layer using spreadsheet. This streamlined approach reduces the lead time from design to fabrication of the device.

4.3. Toolpath Calculation

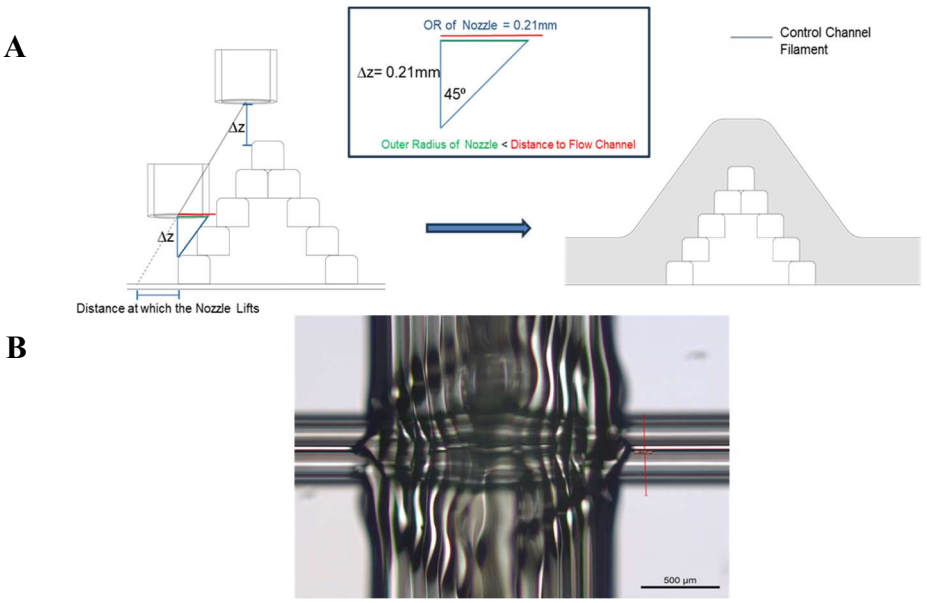

Figure 27. Toolpath calculation (A) Geometric analysis of toolpath calculation (B) Microscopic image of overlap

A calculated toolpath was essential to ensure the precise deposition of silicone filaments conformally over the flow channels. As shown in Fig.27.A., the fixed distance, Δz, between the nozzle and the substrate was set to match the nozzle's outer radius of 0.21 mm. This uniform distance along the triangular slope prevented the nozzle from potentially colliding with already printed flow channels, thanks to the 45-degree angle adopted for printing the flow channels. This angle ensured that the distance from the nozzle's center to the flow channel was consistently greater than the nozzle's radius. Maintaining Δz = 0.21 mm above all points of the flow channel ensured that optimized printing parameters could be used directly.

Geometric calculations determined the point at which the nozzle lifted before approaching the flow channel. By fixing the distance Δz above both the bottommost and topmost filaments, the toolpath was constructed by connecting these points (Fig.27.A.). The resulting line was extended to the substrate to pinpoint the exact lift-off point for the nozzle. This geometrically calculated toolpath method facilitated accurate and conformal printing of control channels over multiple flow channels, ensuring precise alignment and preventing any interference with the printed structures. This technique also held well for designing the toolpath for the downward slope, thanks to the symmetric nature of the isosceles triangle cross-sectioned flow channels. Fig.27.B. shows the microscopic image of the overlap of a control channel over a flow channel that has been accurately printed using the calculated toolpath. The layers of the channels are equally spaced out and maintain the position accurately throughout the length of the control channel.

4.4. 3D Printing System

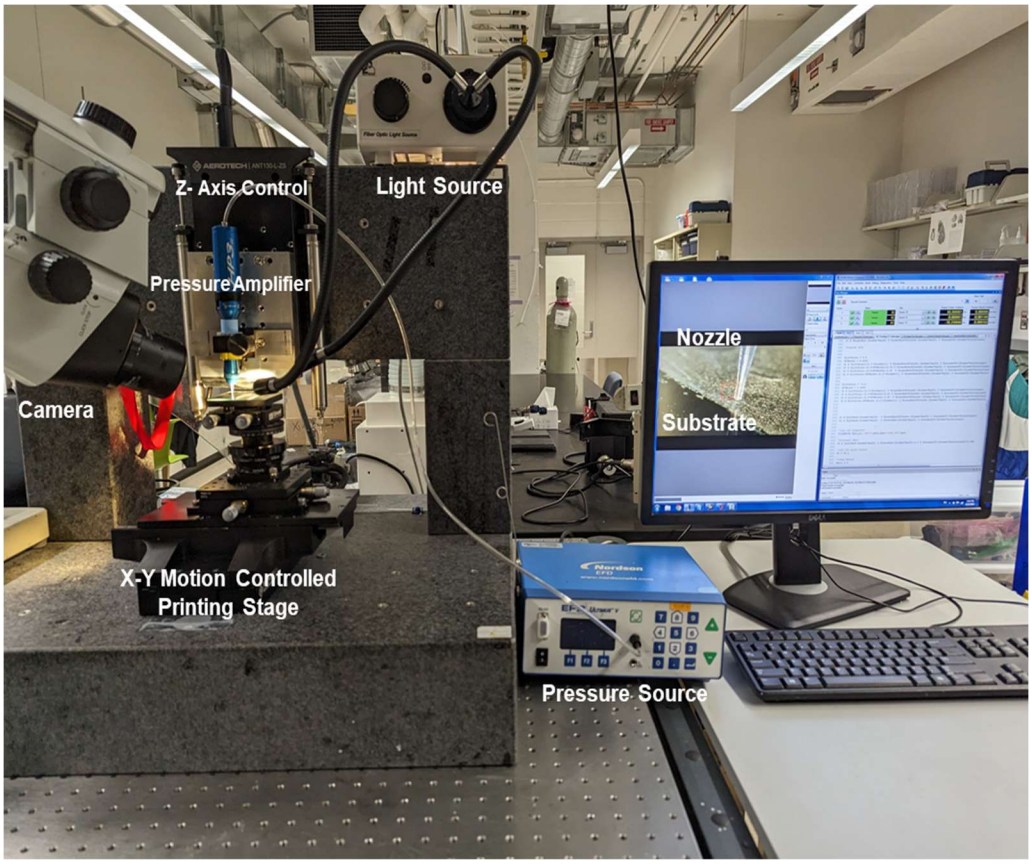

Figure 28. 3D Printing System

Fig.28. shows the 3D printing setup for fabricating for high-density microfluidic devices. A syringe loaded with the required material is connected to a pressure source and placed in the pressure amplification jacket. The pressure makes the barrel push the material out of the syringe. The motion control system (AEROTECH) consists of a moving stage where the substrate is placed. The relative movement of the stage (ANT130XY) with respect to the nozzle, which is stationary in the x-y plane, allows filaments to be patterned onto the required plane. It also consists of a z-axis control (ANT130LZS),

which moves the nozzle along the z-axis to print subsequent layers one over the other. The motion control system is controlled A3200 software (Motion Composer Suite) programmed in G-code, which also sends a signal to the pressure control system to start and stop the extrusion process. A DSLR camera connected to a microscope allows constant monitoring of the miniature prints for observing the real-time printing process to identify process issues such as nozzle clogging and inadequate printing pressures. The initial coordinates are calibrated before the beginning of the printing process, and any required substrate alignments are made using the microscopic camera setup.

4.5. Flow Control Set Up

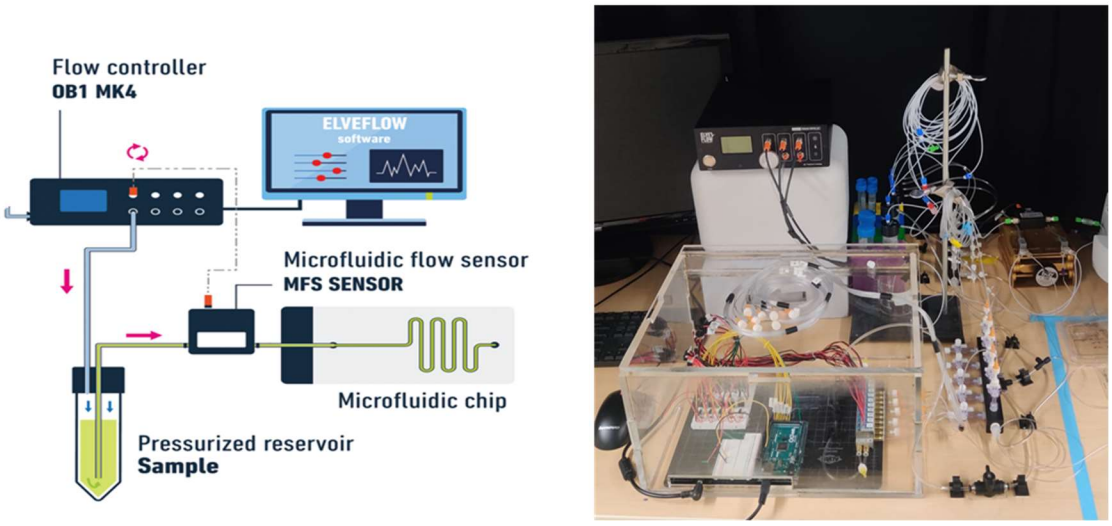

Figure 29. Flow control set up with Arduino controlled piezometric valve system[64]

The characterization of the valves was done with the help of the Elveflow flow controller setup. The first output of the flow controller was pressurized distilled water stored in a

reservoir and connected to the microfluidic channels. This flow was connected to a flow rate sensor, which uses thermal time-of-flight technology to capture real-time data of the flow rate in the fluidic circuit. The second output of the flow controller supplies the actuation pressure of the valve, which is connected to a system of normally open piezometric valves that are controlled using an ARDUINO Mega microcontroller. This system allows constant monitoring of the flow rate data as a response to the actuation pressure supplied to the valves. Tests can be performed by controlling the flow using the sequential flow control interface of Elveflow to program the rate at which the actuation pressure needs to be ramped up or the pressure at which the flow system is set up. A flow resistance wire of diameter 15 µm was also added to the system to avoid fluctuations as the flowrate is highly sensitive to the pressure drop.

4.6. Stress Testing Method

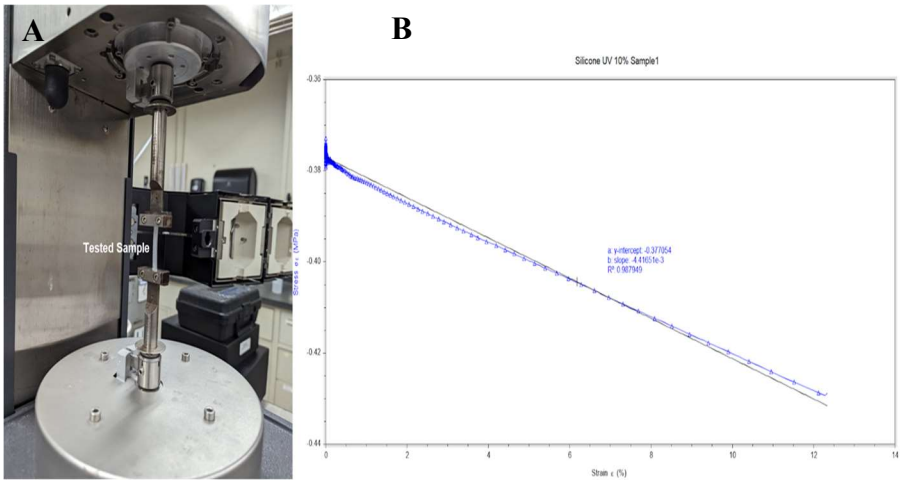

Figure 30. Stress testing method (A) RSA-G2 rheometer setup (B) Result from RSA-G2 tensile testing

To understand the effect of fillers on the mechanical properties of RTV Silicone, rectangular patches (37 mm x 4 mm x 0.8 mm) made of these materials were 3D printed. These patches were securely clamped onto a solid-state rheometer for tensile testing (Fig.30.A.). The rheometer, equipped with a motor for inducing deflection and transducer technology for stress measurement, allowed precise data collection with independent control of these systems. A strain rate of 0.5 mm/s was applied to measure the stress response, and testing occurred within the linear range of the stress-strain curve to determine Young's modulus. Post-data collection, the negative slope of the curve (Fig.30.B.) was calculated to determine Young's modulus of the printed samples, providing insights into the enhanced mechanical properties of channels printed with additives.

4.7. Gradient Generator Simulation Details

The concentration profile of the gradient generator was simulated with the help of finite element analysis (FEA) using COMSOL Multiphysics. A steady state study was carried out using the laminar flow module, simulated using the continuity and momentum conservation equations (equations 1 and 2) of the fluid and the transport of dilute species module simulated by the convection-diffusion equation (equation 3).

$$\nabla \cdot v = 0 \tag{1}$$

$$\frac{\partial v}{\partial t} + (v \cdot \nabla)v = -\frac{1}{\rho}\nabla p + \nu\nabla^2 2v \tag{2}$$

$$\frac{\partial \phi}{\partial t} + v \cdot \nabla\phi - D\phi = 0 \tag{3}$$

The CAD drawing of the gradient generator was exported from SolidWorks as a DXF file and extruded using the CAD tool of the COMSOL Multiphysics software to realize the 3D simulation of the flow and concentration. The boundary conditions of the inlets were set to a flow rate of 10 µl/min and of 0 mol/m3 and 1 mol/m3 for both the inlets were set. The simulation was run, and the concentration at the outlets was determined to calculate the percentage of the concentration achieved from diluting the 1 mol/m^3 flow.

4.8. Bacteria Experiment Set Up

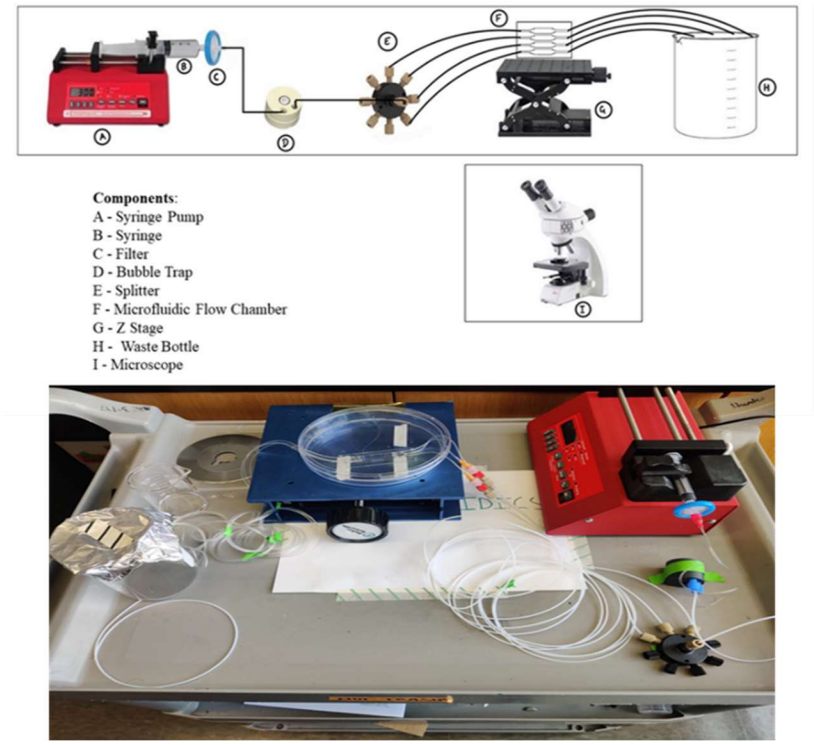

Figure 31. Growing PA14 biofilm in culture chamber

Preliminary experiments were conducted to determine the viability of cultivating biofilms by inoculating them with a liquid bacteria culture. The setup included a syringe pump, which was loaded with the required reagents and manually switched based on the defined protocol. Fig.31.A. shows the illustration of the components of the system, and Fig.31.B. shows the image of the actual biofilm cultivation setup. The syringe pump was loaded with a syringe containing the reagents for the experiment. The loaded syringes were manually switched as required. A 0.45 µm filter was used to remove any external

deposits in the media from entering the flow chamber. This was connected to a bubble trap apparatus to solve the issue of bubbles being introduced into the microfluidic setup that can clog the flow. The flow line could be split into multiple chambers as required by the flow splitter and connected to the 3D-printed microfluidic device where the biofilm was cultivated. The flow from the system was drained into a waste bottle. The system was maintained at a constant flow of nutrient-rich LB broth at 11 µl/min.

4.9. Liquid Culture of PA14 for Inoculation

Pseudomonas aeruginosa (PA14) isolation agar with gentamicin sulfate, a stock solution of 0.01M gentamicin sulfate was created by dissolving 0.516 g of gentamicin sulfate (Amresco) in 100 mL of MilliQ water, which was then filter-sterilized using a 0.22 µm filter to remove large particulates before inoculating into a microfluidic device to ensure clarity for microscopic observation. For the agar medium, 250 mL of MilliQ water was added to a flask along with *Pseudomonas aeruginosa* (PA14) isolation agar, which was autoclaved at 121°C for 30 minutes. Subsequently, 1.2 mL of the 0.01M gentamicin solution was added. YFP tagged PA14 was streaked out on the plates and incubated aerobically overnight at 37°C. A yellow colony was selected and grown in LB + gentamicin. To make the liquid culture of YFP PA 14, 240 µL of the 0.01M gentamicin sulfate stock solution was added to 50 mL of LB, inoculated with YFP PA14, and placed in a shaker for growth.

REFERENCES

[1] I. E. Araci and P. Brisk, "Recent developments in microfluidic large scale integration," *Curr. Opin. Biotechnol.*, vol. 25, pp. 60–68, Feb. 2014, doi: 10.1016/j.copbio.2013.08.014.

[2] A. K. White *et al.*, "High-throughput microfluidic single-cell RT-qPCR," *Proc. Natl. Acad. Sci.*, vol. 108, no. 34, pp. 13999–14004, Aug. 2011, doi: 10.1073/pnas.1019446108.

[3] X. Wu *et al.*, "In situ characterization of the mTORC1 during adipogenesis of human adult stem cells on chip," *Proc. Natl. Acad. Sci.*, vol. 113, no. 29, pp. E4143–E4150, Jul. 2016, doi: 10.1073/pnas.1601207113.

[4] D. D. Liu and L. F. Cheow, "Rapid Information Retrieval from DNA Storage with Microfluidic Very Large-Scale Integration Platform," *Small*, vol. n/a, no. n/a, p. 2309867, doi: 10.1002/smll.202309867.

[5] T. Thorsen, S. J. Maerkl, and S. R. Quake, "Microfluidic Large-Scale Integration," *Science*, vol. 298, no. 5593, pp. 580–584, Oct. 2002, doi: 10.1126/science.1076996.

[6] F. Cui, M. Rhee, A. Singh, and A. Tripathi, "Microfluidic Sample Preparation for Medical Diagnostics," *Annu. Rev. Biomed. Eng.*, vol. 17, no. 1, pp. 267–286, 2015, doi: 10.1146/annurev-bioeng-071114-040538.

[7] A. R. Vollertsen *et al.*, "Modular operation of microfluidic chips for highly parallelized cell culture and liquid dosing via a fluidic circuit board," *Microsyst. Nanoeng.*, vol. 6, no. 1, Art. no. 1, Nov. 2020, doi: 10.1038/s41378-020-00216-z.

[8] T. S. Santisteban, O. Rabajania, I. Kalinina, S. Robinson, and M. Meier, "Rapid spheroid clearing on a microfluidic chip," *Lab. Chip*, vol. 18, no. 1, pp. 153–161, 2018, doi: 10.1039/C7LC01114H.

[9] N. S. G. K. Devaraju and M. A. Unger, "Pressure driven digital logic in PDMS based microfluidic devices fabricated by multilayer soft lithography," *Lab. Chip*, vol. 12, no. 22, pp. 4809–4815, 2012, doi: 10.1039/C2LC21155F.

[10] E. C. Jensen, A. M. Stockton, T. N. Chiesl, J. Kim, A. Bera, and R. A. Mathies, "Digitally programmable microfluidic automaton for multiscale combinatorial mixing and sample processing," *Lab. Chip*, vol. 13, no. 2, pp. 288–296, 2013, doi: 10.1039/C2LC40861A.

[11] Y. Zhou, Z. Yu, M. Wu, Y. Lan, C. Jia, and J. Zhao, “Single-cell sorting using integrated pneumatic valve droplet microfluidic chip,” *Talanta*, vol. 253, p. 124044, Feb. 2023, doi: 10.1016/j.talanta.2022.124044.

[12] Y. Zeng, M. Shin, and T. Wang, “Programmable active droplet generation enabled by integrated pneumatic micropumps,” *Lab. Chip*, vol. 13, no. 2, pp. 267–273, 2013, doi: 10.1039/C2LC40906B.

[13] K. Raj M and S. Chakraborty, “PDMS microfluidics: A mini review,” *J. Appl. Polym. Sci.*, vol. 137, no. 27, p. 48958, 2020, doi: 10.1002/app.48958.

[14] J. Zhou, D. A. Khodakov, A. V. Ellis, and N. H. Voelcker, “Surface modification for PDMS-based microfluidic devices,” *ELECTROPHORESIS*, vol. 33, no. 1, pp. 89–104, 2012, doi: 10.1002/elps.201100482.

[15] X. Li *et al.*, “Desktop aligner for fabrication of multilayer microfluidic devices,” *Rev. Sci. Instrum.*, vol. 86, no. 7, p. 075008, Jul. 2015, doi: 10.1063/1.4927197.

[16] R. Su, F. Wang, and M. C. McAlpine, “3D printed microfluidics: advances in strategies, integration, and applications,” *Lab. Chip*, vol. 23, no. 5, pp. 1279–1299, 2023, doi: 10.1039/D2LC01177H.

[17] A. K. Au, N. Bhattacharjee, L. F. Horowitz, T. C. Chang, and A. Folch, “3D-printed microfluidic automation,” *Lab. Chip*, vol. 15, no. 8, pp. 1934–1941, 2015, doi: 10.1039/C5LC00126A.

[18] H. Gong, A. T. Woolley, and G. P. Nordin, “High density 3D printed microfluidic valves, pumps, and multiplexers,” *Lab. Chip*, vol. 16, no. 13, pp. 2450–2458, 2016, doi: 10.1039/C6LC00565A.

[19] R. D. Sochol *et al.*, “3D printed microfluidic circuitry via multijet-based additive manufacturing,” *Lab. Chip*, vol. 16, no. 4, pp. 668–678, 2016, doi: 10.1039/C5LC01389E.

[20] T. Ching, Y. Li, R. Karyappa, A. Ohno, Y.-C. Toh, and M. Hashimoto, “Fabrication of integrated microfluidic devices by direct-ink-writing (DIW) 3D printing,” *Sens. Actuators B Chem.*, vol. 297, p. 126609, Oct. 2019, doi: 10.1016/j.snb.2019.05.086.

[21] R. Su *et al.*, “3D printed self-supporting elastomeric structures for multifunctional microfluidics,” *Sci. Adv.*, vol. 6, no. 41, p. eabc9846, Oct. 2020, doi: 10.1126/sciadv.abc9846.

[22] C. M. Benjamin Ho, S. Huan Ng, K. H. Holden Li, and Y.-J. Yoon, “3D printed microfluidics for biological applications,” *Lab. Chip*, vol. 15, no. 18, pp. 3627–3637, 2015, doi: 10.1039/C5LC00685F.

[23] A. Colas and J. Curtis, “7 - Silicones,” in *Handbook of Polymer Applications in Medicine and Medical Devices*, K. Modjarrad and S. Ebnesajjad, Eds., in Plastics Design Library. , Oxford: William Andrew Publishing, 2013, pp. 131–143. doi: 10.1016/B978-0-323-22805-3.00007-4.

[24] M. A. Unger, H.-P. Chou, T. Thorsen, A. Scherer, and S. R. Quake, “Monolithic Microfabricated Valves and Pumps by Multilayer Soft Lithography,” *Science*, vol. 288, no. 5463, pp. 113–116, Apr. 2000, doi: 10.1126/science.288.5463.113.

[25] Y.-S. Lee, N. Bhattacharjee, and A. Folch, “3D-printed Quake-style microvalves and micropumps,” *Lab. Chip*, vol. 18, no. 8, pp. 1207–1214, 2018, doi: 10.1039/C8LC00001H.

[26] C. I. Rogers, K. Qaderi, A. T. Woolley, and G. P. Nordin, “3D printed microfluidic devices with integrated valves,” *Biomicrofluidics*, vol. 9, no. 1, p. 016501, Jan. 2015, doi: 10.1063/1.4905840.

[27] H. Gong, B. P. Bickham, A. T. Woolley, and G. P. Nordin, “Custom 3D printer and resin for 18 μm × 20 μm microfluidic flow channels,” *Lab. Chip*, vol. 17, no. 17, pp. 2899–2909, 2017, doi: 10.1039/C7LC00644F.

[28] A. D. Castiaux, M. A. Selemani, M. A. Ward, and R. Scott Martin, “Fully 3D printed fluidic devices with integrated valves and pumps for flow injection analysis,” *Anal. Methods*, vol. 13, no. 42, pp. 5017–5024, 2021, doi: 10.1039/D1AY01569A.

[29] M. P. de Beer, H. L. van der Laan, M. A. Cole, R. J. Whelan, M. A. Burns, and T. F. Scott, “Rapid, continuous additive manufacturing by volumetric polymerization inhibition patterning,” *Sci. Adv.*, vol. 5, no. 1, p. eaau8723, Jan. 2019, doi: 10.1126/sciadv.aau8723.

[30] H. K. Park, M. Shin, B. Kim, J. W. Park, and H. Lee, “A visible light-curable yet visible wavelength-transparent resin for stereolithography 3D printing,” *NPG Asia Mater.*, vol. 10, no. 4, Art. no. 4, Apr. 2018, doi: 10.1038/s41427-018-0021-x.

[31] A. K. Au, N. Bhattacharjee, L. F. Horowitz, T. C. Chang, and A. Folch, “3D-printed microfluidic automation,” *Lab. Chip*, vol. 15, no. 8, pp. 1934–1941, 2015, doi: 10.1039/C5LC00126A.

[32] J. L. Sanchez Noriega *et al.*, “Spatially and optically tailored 3D printing for highly miniaturized and integrated microfluidics,” *Nat. Commun.*, vol. 12, no. 1, Art. no. 1, Sep. 2021, doi: 10.1038/s41467-021-25788-w.

[33] H. Yuk and X. Zhao, “A New 3D Printing Strategy by Harnessing Deformation, Instability, and Fracture of Viscoelastic Inks,” *Adv. Mater.*, vol. 30, no. 6, p. 1704028, 2018, doi: 10.1002/adma.201704028.

[34] R. Tu and H. A. Sodano, “Additive manufacturing of high-performance vinyl ester resin via direct-ink-writing with UV-thermal dual curing,” *Addit. Manuf.*, vol. 46, p. 102180, Oct. 2021, doi: 10.1016/j.addma.2021.102180.

[35] A. Z. Nelson, K. S. Schweizer, B. M. Rauzan, R. G. Nuzzo, J. Vermant, and R. H. Ewoldt, “Designing and transforming yield-stress fluids,” *Curr. Opin. Solid State Mater. Sci.*, vol. 23, no. 5, p. 100758, Oct. 2019, doi: 10.1016/j.cossms.2019.06.002.

[36] M. a. S. R. Saadi *et al.*, “Direct-ink-writing: A 3D Printing Technology for Diverse Materials,” *Adv. Mater.*, vol. 34, no. 28, p. 2108855, 2022, doi: 10.1002/adma.202108855.

[37] Y. Wang and N. Willenbacher, “Phase-Change-Enabled, Rapid, High-Resolution Direct-ink-writing of Soft Silicone,” *Adv. Mater.*, vol. 34, no. 15, p. 2109240, 2022, doi: 10.1002/adma.202109240.

[38] S. Malek, J. R. Raney, J. A. Lewis, and L. J. Gibson, “Lightweight 3D cellular composites inspired by balsa,” *Bioinspir. Biomim.*, vol. 12, no. 2, p. 026014, Mar. 2017, doi: 10.1088/1748-3190/aa6028.

[39] C. Mo, R. Yin, and J. R. Raney, “Direct-ink-writing of tough, stretchable silicone composites,” *Soft Matter*, vol. 18, no. 38, pp. 7341–7347, 2022, doi: 10.1039/D2SM00923D.

[40] J. L. Erkal *et al.*, “3D printed microfluidic devices with integrated versatile and reusable electrodes,” *Lab. Chip*, vol. 14, no. 12, pp. 2023–2032, 2014, doi: 10.1039/C4LC00171K.

[41] D. Therriault, S. R. White, and J. A. Lewis, “Chaotic mixing in three-dimensional microvascular networks fabricated by direct-write assembly,” *Nat. Mater.*, vol. 2, no. 4, Art. no. 4, Apr. 2003, doi: 10.1038/nmat863.

[42] V. Saggiomo and A. H. Velders, “Simple 3D Printed Scaffold-Removal Method for the Fabrication of Intricate Microfluidic Devices,” *Adv. Sci.*, vol. 2, no. 9, p. 1500125, 2015, doi: 10.1002/advs.201500125.

[43] E. A. Cherney, “RTV silicone-a high tech solution for a dirty insulator problem,” *IEEE Electr. Insul. Mag.*, vol. 11, no. 6, pp. 8–14, Nov. 1995, doi: 10.1109/57.475903.

[44] F. White, *Viscous Fluid Flow.* Boston: McGraw-Hill. 2nd ed., 1991.

[45] G. Ferreira, A. Sucena, L. L. Ferrás, F. T. Pinho, and A. M. Afonso, “Hydrodynamic Entrance Length for Laminar Flow in Microchannels with Rectangular Cross Section,” *Fluids*, vol. 6, no. 7, Art. no. 7, Jul. 2021, doi: 10.3390/fluids6070240.

[46] H. A. Stone and S. Kim, “Microfluidics: Basic issues, applications, and challenges,” *Am. Inst. Chem. Eng. AIChE J.*, vol. 47, no. 6, p. 1250, Jun. 2001.

[47] H. Sugioka, “Chaotic mixer using electro-osmosis at finite P\’eclet number,” *Phys. Rev. E*, vol. 81, no. 3, p. 036306, Mar. 2010, doi: 10.1103/PhysRevE.81.036306.

[48] J. Bem You *et al.*, “PDMS-based turbulent microfluidic mixer,” *Lab. Chip*, vol. 15, no. 7, pp. 1727–1735, 2015, doi: 10.1039/C5LC00070J.

[49] J. Marschewski *et al.*, “Mixing with herringbone-inspired microstructures: overcoming the diffusion limit in co-laminar microfluidic devices,” *Lab. Chip*, vol. 15, no. 8, pp. 1923–1933, 2015, doi: 10.1039/C5LC00045A.

[50] J. Marschewski *et al.*, “Mixing with herringbone-inspired microstructures: overcoming the diffusion limit in co-laminar microfluidic devices,” *Lab. Chip*, vol. 15, no. 8, pp. 1923–1933, 2015, doi: 10.1039/C5LC00045A.

[51] P. J. Schmid and D. S. Henningson, “Optimal energy density growth in Hagen–Poiseuille flow,” *J. Fluid Mech.*, vol. 277, pp. 197–225, Oct. 1994, doi: 10.1017/S0022112094002739.

[52] B. J. Kirby, *Micro- and Nanoscale Fluid Mechanics: Transport in Microfluidic Devices*. Cambridge University Press, 2010.

[53] K. W. Oh, K. Lee, B. Ahn, and E. P. Furlani, “Design of pressure-driven microfluidic networks using electric circuit analogy,” *Lab. Chip*, vol. 12, no. 3, pp. 515–545, 2012, doi: 10.1039/C2LC20799K.

[54] W. H. Hayt, J. E. Kemmerly, and S. M. Durbin, *Engineering Circuit Analysis*, 8th edn. McGraw-Hill, New York, 2012.

[55] K. Lee *et al.*, “Generalized serial dilution module for monotonic and arbitrary microfluidic gradient generators,” *Lab. Chip*, vol. 9, no. 5, pp. 709–717, 2009, doi: 10.1039/B813582G.

[56] J. W. Costerton, Z. Lewandowski, D. E. Caldwell, D. R. Korber, and H. M. Lappin-Scott, “Microbial biofilms,” *Annu. Rev. Microbiol.*, vol. 49, pp. 711–747, Jan. 1995.

[57] C. Beloin, A. Roux, and J.-M. Ghigo, “Escherichia coli Biofilms,” in *Bacterial Biofilms*, T. Romeo, Ed., in Current Topics in Microbiology and Immunology. , Berlin, Heidelberg: Springer, 2008, pp. 249–289. doi: 10.1007/978-3-540-75418-3_12.

[58] A. Persat *et al.*, “The Mechanical World of Bacteria,” *Cell*, vol. 161, no. 5, pp. 988–997, May 2015, doi: 10.1016/j.cell.2015.05.005.

[59] J. S. Guasto, R. Rusconi, and R. Stocker, “Fluid Mechanics of Planktonic Microorganisms,” *Annu. Rev. Fluid Mech.*, vol. 44, no. 1, pp. 373–400, 2012, doi: 10.1146/annurev-fluid-120710-101156.

[60] R. Rusconi, M. Garren, and R. Stocker, “Microfluidics Expanding the Frontiers of Microbial Ecology,” *Annu. Rev. Biophys.*, vol. 43, no. 1, pp. 65–91, 2014, doi: 10.1146/annurev-biophys-051013-022916.

[61] P. Bourke, D. Ziuzina, L. Han, P. J. Cullen, and B. F. Gilmore, “Microbiological interactions with cold plasma,” *J. Appl. Microbiol.*, vol. 123, no. 2, pp. 308–324, Aug. 2017, doi: 10.1111/jam.13429.

[62] L. Han, D. Boehm, S. Patil, P. J. Cullen, and P. Bourke, “Assessing stress responses to atmospheric cold plasma exposure using Escherichia coli knock-out mutants,” *J. Appl. Microbiol.*, vol. 121, no. 2, pp. 352–363, Aug. 2016, doi: 10.1111/jam.13172.

[63] J. Kim, M. Hegde, S. Ho Kim, T. K. Wood, and A. Jayaraman, “A microfluidic device for high throughput bacterial biofilm studies,” *Lab. Chip*, vol. 12, no. 6, pp. 1157–1163, 2012, doi: 10.1039/C2LC20800H.

[64] “Autonomous microfluidic pump,” Elveflow. [Online]. Available: https://www.elveflow.com/microfluidic-products/microfluidics-flow-control-systems/autonomous-vacuum-pressure-pumps/z

APPENDIX

Relevant files such as G-Codes, Results, and CAD Files are stored in the following drive link.

https://drive.google.com/drive/folders/17NM_gW6fRJi5ojYr8UMNFXj-ehANNJuj?usp=drive_link